Computer Based On-line Diagnostics of Insulation Quality of High Voltage Apparatus

by

Pei Wang

A Thesis

Submitted to the Faculty of Graduate Studies

in partial fulfillment of the requirements

for the degree of

Master of Science

Department of Electrical and Computer Engineering

University of Manitoba

Winnipeg, Manitoba, Canada

THE UNIVERSITY OF MANITOBA

FACULTY OF GRADUATE STUDIES

*****

COPYRIGHT PERMISSION PAGE

Computer Based On-Line Diagnostics of Insulation Quality of High Voltage Apparatus

BY

Pei Wang

A Thesis/Practicum submitted to the Faculty of Graduate Studies of The University of Manitoba in partial fulfillment of the requirements of the degree of M.SC

Acknowledgements

First of all I would like to express my profound gratitude to Dr. M.R. Raghuveer. Throughout this whole work, Dr. M.R. Raghuveer gave me invaluable guidance and advice. His intelligence, wisdom, modesty and personality have been an inspiration to me ever since I met him.

I wish to express my sincere thanks to Mr. W. McDermid and Mr. Jim Bromley of Manitoba Hydro for their valuable advice and help.

Funding from Manitoba Hydro made available by the Manitoba Hydro Research Committee is gratefully appreciated.

Special thanks to Mr. John Kendall, the technician in the McMath High Voltage & Power Transmission Research Laboratory at University of Manitoba, for his technical support in the experiments and his friendship.

Finally, I would like to express my deeply appreciation to my wife, Jingxuan and my family for their love, encouragement and support during the period of my study.

Abstract

The safe and reliable operation of a power system is directly related to the insulation condition of high voltage apparatus in service, which may age and deteriorate under normal operating conditions. Therefore, the detection of insulation quality of high voltage apparatus is important. This task can be implemented advantageously by the measurement of dissipation factor and capacitance using on-line digital methods, since these methods require no service interruption thus resulting in low labor cost. Moreover, on-line measurements under operating voltage are more helpful in the assessment of the status of the insulation.

In this work, a computer-aided system for on-line monitoring dissipation factor and capacitance was developed based on a method, which employs the Discrete Fourier Transform (DFT). The DFT is performed on the scaled down analog voltage and current signals obtained using a Digital Storage Oscilloscope (DSO) board, and results are displayed using the graphic user interface which is implemented with software Labview. To optimize system performance, software simulation and laboratory tests were carried out. Based on the results, optimal values of measurement parameters have been suggested. Field tests were conducted at Manitoba Hydro' s Dorsey station to evaluate the insulation of a 230KV current transformer unit using the developed system.

Table of Contents

List of Figures

List of Tables

CHAPTER 1

INTRODUCTION

1.1 A Brief History of Insulation Diagnostic Methods

The safe and reliable operation of a power system is directly related to the insulation condition of high voltage apparatus in service. Generally, high voltage insulation ages and deteriorates under normal operating conditions, and this process may be accelerated due to the effects of lighting and switching overvoltages, large temperature changes, and moisture ingress. To avoid insulation failure and its damaging effects, several diagnostic methods have been developed over the years which may be divided into two categories, i.e. non-destructive and destructive tests. These tests can be implemented electrically, physically or chemically.

Widely adopted non-destructive methods include dissipation factor and capacitance measurement, partial discharge detection, insulation resistance measurement, dissolved gas analysis and the voltage recovery method [1-3]. The test procedure and criteria used to detect insulation degradation have been standardized, and these methods have proved to be effective laboratory methods. However, the implementation of these methods requires removal of equipment from service and therefore service interruption. Moreover, the time-based maintenance does not depend on the real insulation condition of the equipment resulting in some unnecessary tests and cost. In addition, test conditions require controls for the repeatability of the test results.

With the development of digital technologies, it has become possible to realize on-line methods, which may be used to detect the insulation quality of high voltage apparatus under operating conditions. On-line methods have been used for the measurement of partial discharge and dielectric loss, and applied to apparatus such as transformers, high voltage bushing and cables [4-6]. However, on-line methods are still in the development stage; new technologies are needed and more data have to be collected to accomplish the main objective, i.e. building an expert system to diagnose the condition of the equipment according to certain criteria.

1.2 Characteristic Parameters Representing Insulation Quality

The insulation of power apparatus is usually modelled as a capacitor, whose quality is influenced by the condition of its dielectric. Ideally, if the capacitor is lossless, the phase shift between voltage and current is exactly 90 degrees under ac voltage. However, dielectric loss does exist because of the finite resistance of the dielectric, polarization loss and occurrence of partial discharges under high voltage. Therefore, practical insulation systems are represented by a RC combination either in series or in parallel. Fig. 1.1 shows the equivalent circuits and phasor diagrams. Clearly, the power factor angle φ is less than 90 degrees, and the complement of the power factor angle, δ, is the well-known loss angle. For both the series and parallel representations, the tangent of loss angle, dissipation factor ($\tan\delta$) can be expressed as

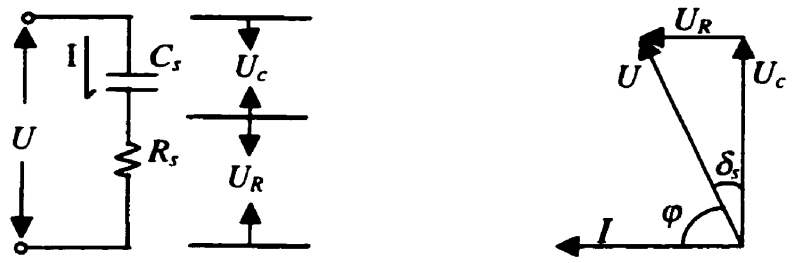

(a) Series circuit

(b) Parallel circuit

Figure 1.1 Equivalent circuits and phasor diagrams of dielectric with loss

$$\tan\delta_s = \frac{U_r}{U_c} = \frac{IR_s}{I * \frac{1}{\omega C_s}} = \omega R_s C_s \tag{1-1}$$

$$\tan\delta_p = \frac{I_r}{I_c} = \frac{U/R_p}{U\omega C_p} = \frac{1}{\omega R_p C_p} \tag{1-2}$$

For good quality insulation, there is not much difference between C_p and C_s, and the relationship between them can be expressed as:

$$C_p = \frac{C_s}{1+\tan^2\delta}; \tag{1-3}$$

The dissipation factor, tanδ, is a measure of dielectric losses, a key parameter representing insulation condition. Usually, tanδ values are small for good insulation, while poor insulation, where the dielectric has deteriorated or is damaged, is associated

with two changes [7]. One is the increased dielectric losses (I^2R), i.e. increased tanδ values, and the other is increased sensitivity to changes in temperature, which is reflected in tanδ as follows:

$$\tan\delta_2 = \tan\delta_1 * e^{\alpha(T_2 - T_1)} \qquad (1\text{-}4)$$

In Eq. 1.4, $\tan\delta_1$ and $\tan\delta_2$ are the values at temperatures T_1 and T_2 respectively, and α is the temperature coefficient depending on the type, size, and condition of insulation. Fig. 1.2 shows the typical dependence of tanδ values on temperature.

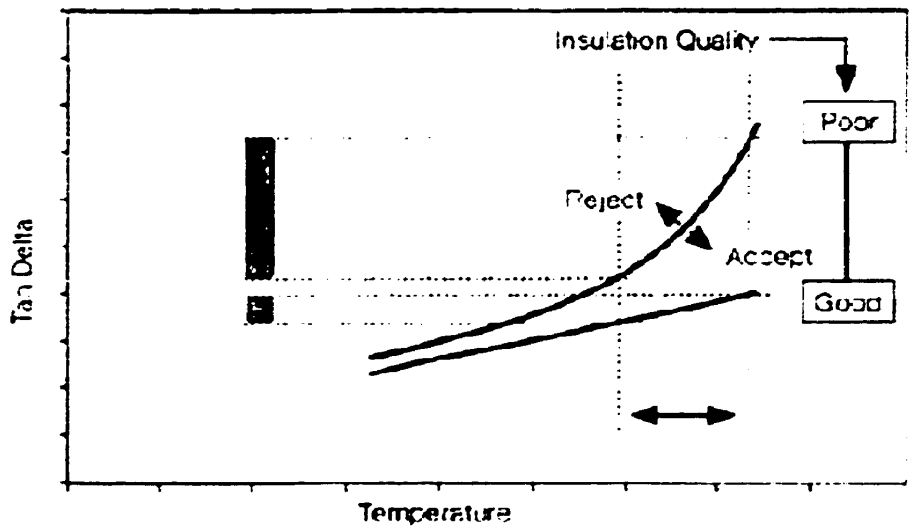

Figure 1.2 Variation of tanδ with temperature
illustrates sensitivity to temperature changes for poor insulation [7]

Therefore, the important information of real insulation condition can be obtained by measuring tanδ values or its change with respect to other parameters such as temperature, together with another important parameter, the capacitance of the insulation.

1.3 Tanδ and Capacitance Measurement Method

1.3.1 Conventional Methods

1.3.1.1 Schering Bridge

The Schering bridge method is commonly employed for the precise measurement of tanδ and capacitance. The basic arrangement in the Schering bridge method is shown in Fig. 1.3. The insulation condition is modelled as a parallel combination Z_x (R_x, C_x). In the circuit, Z_3 and Z_4 are adjustable with high measurement precision, while Z_0 (C_0) is a gas filled standard capacitor whose dielectric loss angle may be assumed as zero. G is the null detector.

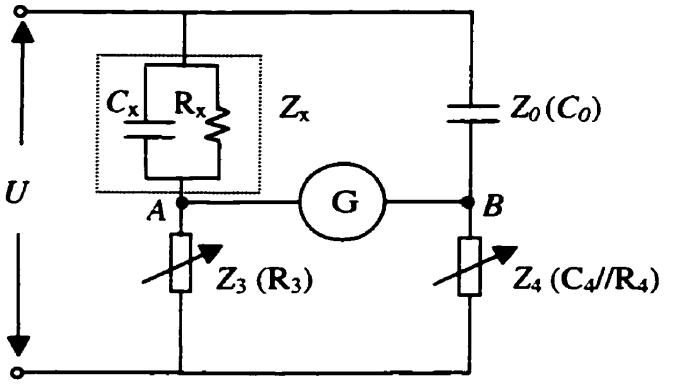

Figure 1.3 Measurement arrangement of Schering bridge method

The principle of this method is to compare and balance the voltages at points A and B (phase and magnitude) of the two branches, i.e. Z_x-Z_3 and Z_0-Z_4. The basic equation under balance condition is shown as

$$\frac{Z_x}{Z_3} = \frac{Z_0}{Z_4}, \tag{1-5}$$

where Z_3, Z_0 ,Z_4 and Zx are the corresponding impedances.

From the above equation,

$$\tan\delta = \frac{1}{\omega C_x R_x} = \omega C_4 R_4$$

$$C_x = \frac{C_0 R_4}{R_3} * \frac{1}{(1-\tan^2\delta)} \approx \frac{C_0 R_4}{R_3} \qquad (1\text{-}6)$$

In the Schering bridge method, measurement errors arise mainly due to stray capacitance of the branches and electromagnetic interference from some high frequency sources. Those problems are minimized by use of the double shielded bridge equipped with a unity gain amplifier [1].

1.3.1.2 Current Comparator

The current comparator may also be used to measure tanδ and capacitance with high precision, and Fig. 1.4 shows the measurement set-up. The main part of the circuit consists of a three-winding current comparator. Different from the Schering bridge method, the current comparator method compares and balances the ampere-turns in the coils to obtain dissipation factor and capacitance.

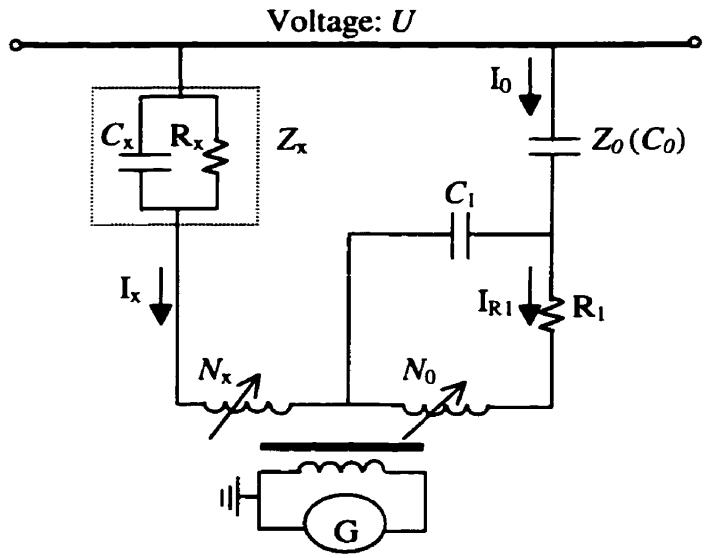

Figure 1.4 Measurement set-up of the current comparator method

The balance condition is

$$N_x I_x = N_0 I_{R1} \tag{1-7}$$

From the above equation,

$$\tan\delta = \omega R_1 (C_0 + C_1)$$
$$C_x = \frac{N_0}{N_x} C_0 \tag{1-8}$$

A significant advantage of this method is that the influence of stray capacitance is eliminated, since they do not enter in the balance condition. Therefore, the current comparator method has higher accuracy than the Schering bridge method.

1.3.2 On-line Methods

Researchers have carried out considerable work concerning the use of on-line methods to measure dissipation factor and capacitance. The methods presented basically utilize the current signals through and/ or the voltage signals across the test objects, while the main difference lies in the manner in which the signals are acquired and the handling of data to obtain the results. These methods can be divided into four categories: modification of conventional comparison methods [7-9], the method employing zero-crossing detection [4][10], sum current method [5], and harmonic analysis method which offers significant advantages [11].

The measurement arrangement in the voltage comparison method is shown in Fig. 1.5. The principle is based on the conventional Schering bridge method used in laboratories around the world. Data acquired under software control from each test object is processed to present tanδ and capacitance measurement.

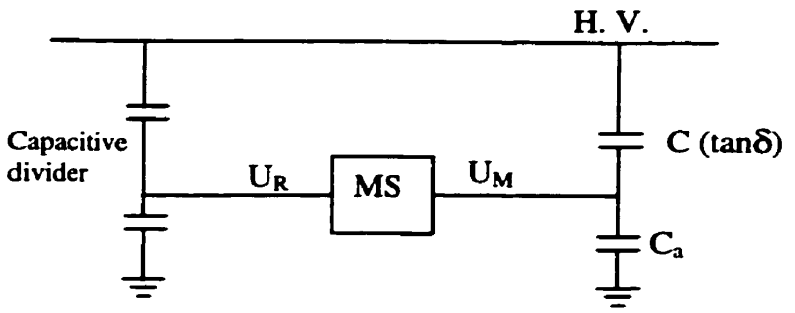

Figure 1.5 Basic arrangement of voltage comparison method [9]

HV-- operating voltage; C-- capacitance of insulation;

C_a -- additional capacitance for signal conditioning

U_R -- reference voltage;

U_M --measurement signal voltage;

MS --monitoring system

Reference [4] describes the method of zero-crossings detection. In this method, the measured current and voltage signals are first converted into rectangular waveforms relying on detection of zero-crossing points; next, a difference pulse is obtained using a logic circuit, as shown in Fig. 1.6. The pulse width contains information about the

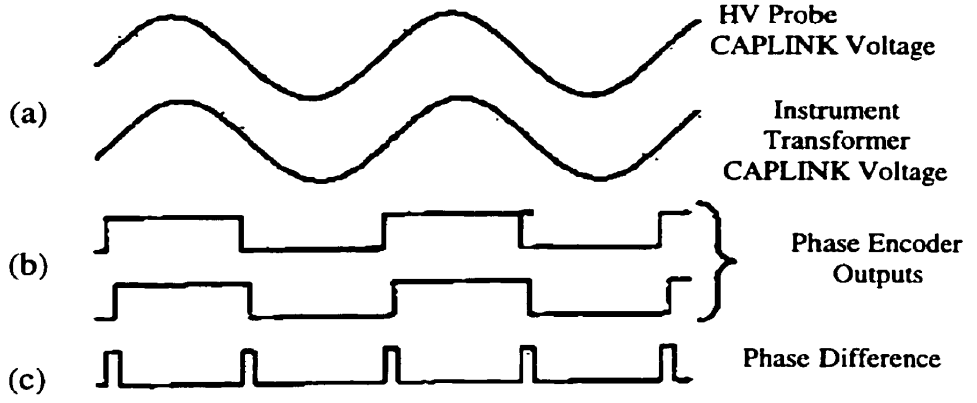

Figure 1.6 Derivation of the difference pulses [4]

phase difference. This method has been used in a substation, and its basic set-up is shown in Fig. 1.7. The errors in this method arise mainly due to noise and harmonics in the power system, and a hardware circuit has to be built to eliminate their effects.

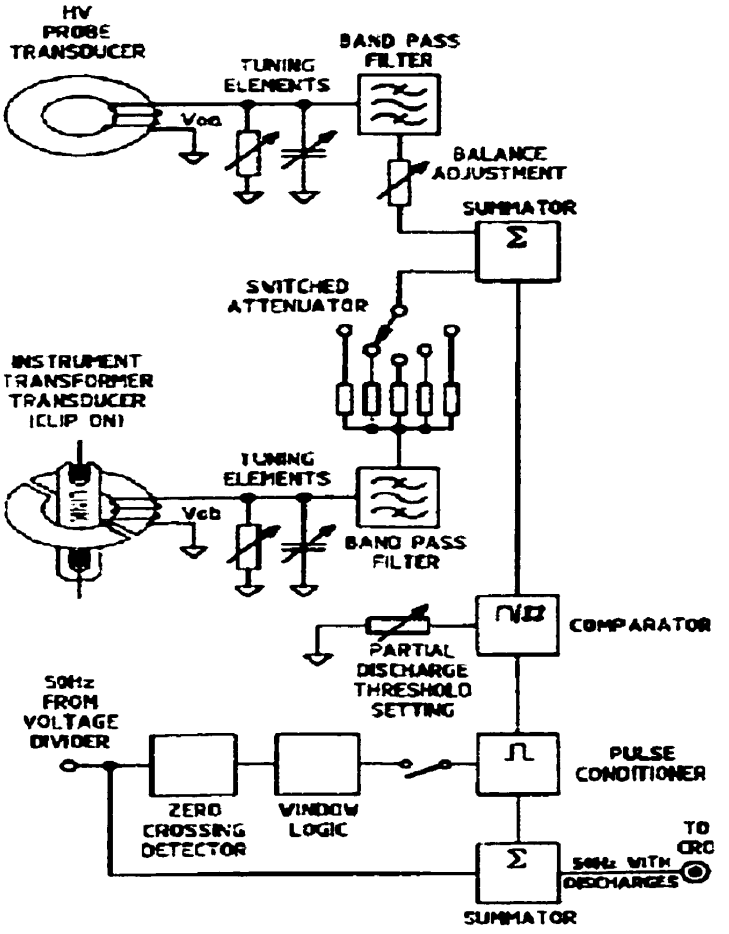

Figure 1.7 Measurement set-up of the zero detection method [4]

Fig. 1.8 shows the basic set-up and phasor diagram of the sum current method [5]. This method is based on summing vectorially the three-phase bushing (or current transformer) capacitive currents, and detecting the imbalance current. For a symmetrical

power system, the sum of the three-phase current will be ideally zero; If the insulation condition of one phase changes, the sum will change too. So the sum current may be used as an indicator of the insulation condition of the high voltage apparatus. An algorithm for calculating the sum current as a function of power factor and capacitance has been developed and the correspondent on-line diagnostics system have been installed at 12 station for 49 bushing and CT units. It is pointed out that further study is necessary to ascertain the influence of ambient temperature, humidity and power system conditions on the sum current behavior.

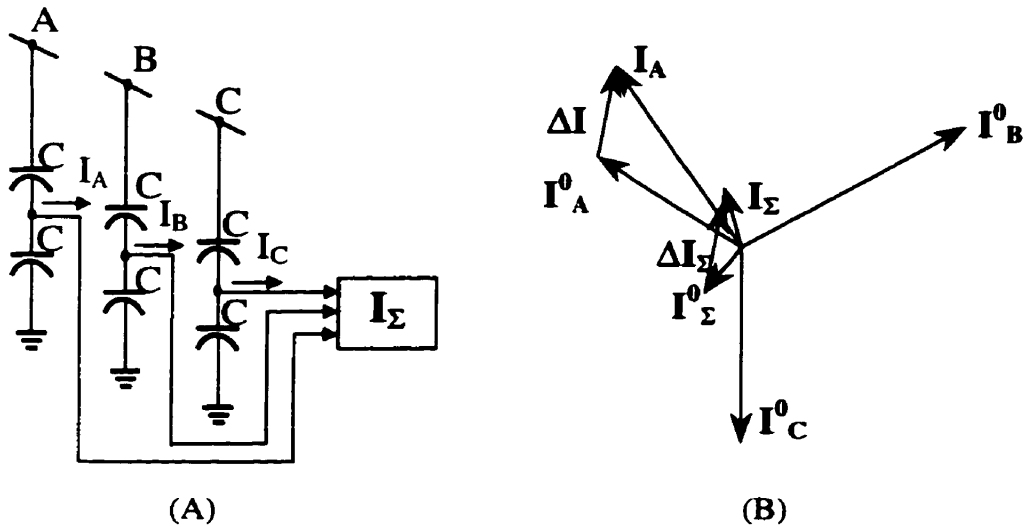

Figure 1.8 Basic set-up and phasor diagram of sum current method [5]

Reference [11] presents the harmonics analysis method using the digital principle, and its schematic diagram of set-up is shown in Fig. 1.9. In this method, the Discrete Fourier Transform (DFT) is performed on the acquired analog voltage and current signals, and the phase difference is found from phase information of the fundamental quantities in the signals.

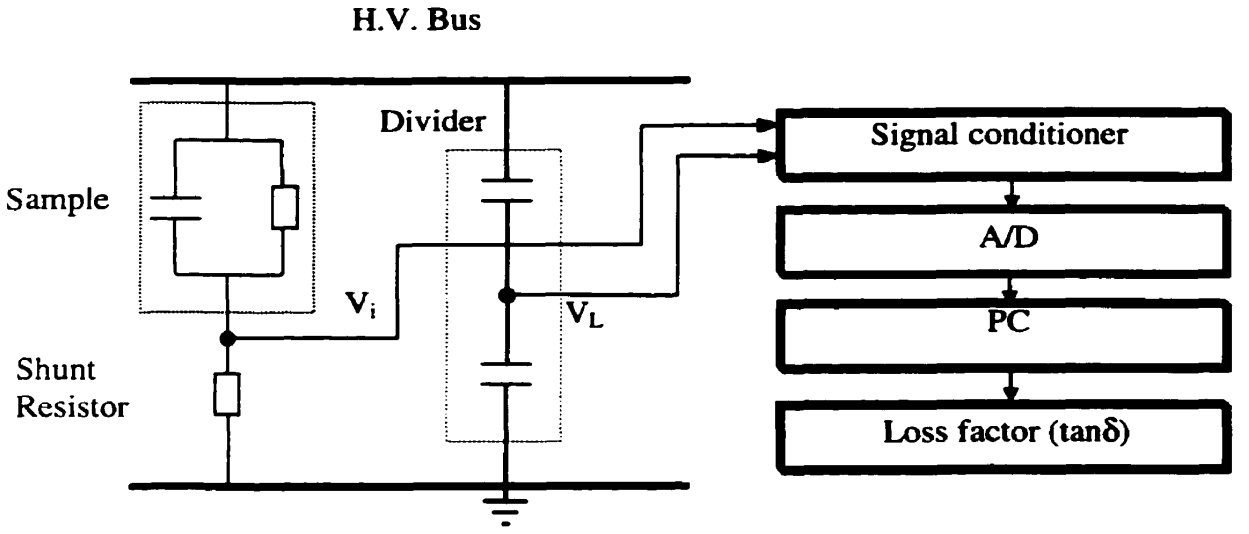

Figure 1.9 Measurement arrangement of harmonic analysis method [11]

1.4 Scope of The Present Work

The scope of the present work is to extend the applicability of the digital method [11] using a computer based instrument, the Digital Storage Oscilloscope (DSO), to measure the dissipation factor and capacitance of high voltage apparatus. The work carried out includes the followings:

- Development of a computer-base measurement system and its graphic user interface (GUI), based on the digital storage oscilloscope board and the programming environment Labview.
- Software simulation to find out the effects of different parameters such as sampling rate, trigger point locations, frequency fluctuation, voltage harmonics, and choice of optimum measurement parameters.

- Investigation of a method which employs cancellation of capacitive current for measuring dissipation factor and capacitance of high capacitance insulation.
- Verification of the developed measurement system by conducting low and high voltage laboratory tests.
- Hardening of the developed system.
- On-line measurement of the insulation of a 230kV current transformer unit at Manitoba Hydro's Dorsey station.

CHAPTER 2

DEVELOPMENT AND VALIDATION OF DIGITAL MEASUREMENT SYSTEM

In this chapter, the principle and components of the digital system for measuring dissipation factor and capacitance of H.V. apparatus are introduced. To optimize system performance, software simulation and laboratory tests were carried out. Based on the results, optimal values of measurement parameters have been suggested. In addition, a method applicable for the measurement of high capacitance insulation is investigated and the results are presented.

2.1 Measurement Method

As discussed in Chapter 1, the voltage signal across the test object, $V_v(t)$ and the signal proportional to the current flowing through the test object, $V_I(t)$ provide information concerning the insulation condition of H.V apparatus. If these signals are pure sinusoidal waveforms then the dielectric loss angle δ of H.V. apparatus can be obtained using the phase information, as shown in Fig. 2.1. However, the practical signal in power system is always contaminated by harmonic components, and the periodic signals $V_v(t)$ and $V_I(t)$ can be represented as in Eq. 2.1 by using Fourier Series.

$$V_v(t) = V_{v0} + \sum_{k=1}^{\infty} V_{vk} * \sin(k\omega t + \theta_{vk})$$

$$V_l(t) = V_{l0} + \sum_{k=1}^{\infty} V_{lk} * \sin(k\omega t + \theta_{lk}) \tag{2-1}$$

where $\omega = 2\pi / T$ is the angular frequency; T represents the period of the signal while k is the harmonic component number.

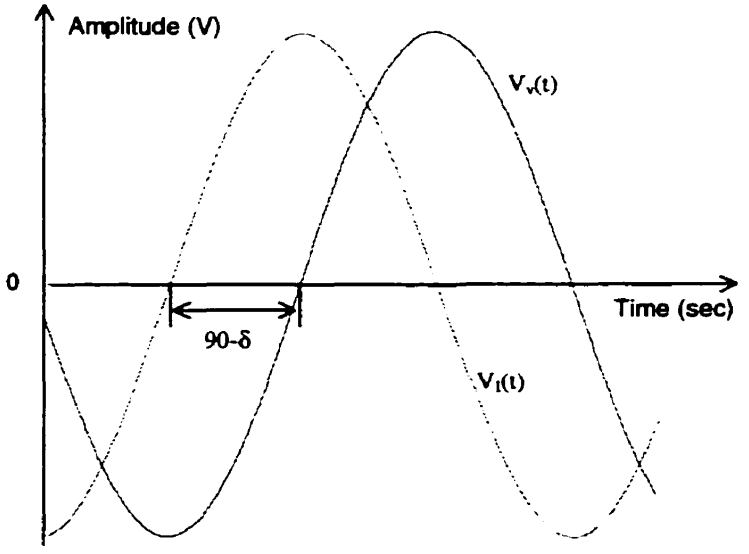

$V_v(t)$: voltage signal waveform
$V_I(t)$: waveform representing current signal

Figure 2.1 Illustration showing the dielectric loss angle, δ

Since the dielectric loss angle is only related to the phase of the fundamental components of the signals, clearly the key of the employed digital method is to eliminate the effects of harmonics and obtain the information from the fundamental components. Generally, this process involves data acquisition and sampling in the time domain, and frequency spectrum analysis using the Discrete Fourier Transform (DFT).

2.1.1 Data Acquisition

To analyze the signal using a digital method, the practical analog signal first has to be converted to the digital form, i.e. a sampled version of the signal, using an analog-to-digital converter. According to the sampling theorem, if the sampling frequency f_s is at least twice the highest frequency f_h in the original signal (Eq.2.2), then we can reconstruct the original signal without the loss of information.

$$f_s \geq 2 * f_h \tag{2-2}$$

Due to electromagnetic interference and other sources, a practical signal usually consists of high frequency components. Therefore, a low-pass filter is employed before data digitization to eliminate effects of the high frequency components. In this work, a signal conditioning circuit provides a low-pass filter with a bandwidth of 10kHZ and the lowest sampling rate used is 25kS/s (S/s denotes samples/Second).

2.1.2 Data Analysis Using DFT

The Discrete Fourier Transform is used to obtain the representation of the finite-length signal (sampled version of the original signal) in the frequency domain. For a finite length signal x[n] defined over the range 0<n<N , the Discrete Fourier Transform of such a signal is given by

$$\begin{aligned} X[k] &= \sum_{n=0}^{k-1} x[n] * \exp(\frac{-j2\pi kn}{N}) \\ &= \sum_{n=0}^{k-1} x[n] * [\cos(\frac{2\pi kn}{N}) - j\sin(\frac{2\pi kn}{N})] \end{aligned} \tag{2-3}$$

For periodic and real signals in a power system, the DFT coefficients X[k] actually

provide the amplitude and phase information of the harmonic components of the original signals. Therefore, the real part $R_e(X[k])$ and imaginary part $I_m(X[k])$ of the DFT coefficients can be shown as the following

$$R_e(X[k]) = \sum_{n=0}^{k-1} x[n] * \cos(\frac{2\pi kn}{N})$$

$$I_m(X[k]) = -\sum_{n=0}^{k-1} x[n] * j\sin(\frac{2\pi kn}{N}) \qquad (2\text{-}4)$$

In terms of the amplitude and phase, these equations can be recast as

$$|X[k]| = [R_e^{\,2}(X[k]) + I_m^{\,2}(X[k])]^{\frac{1}{2}}$$

$$\theta[k] = tg^{-1}[\frac{I_m(X[k])}{R_e(X[k])}] \qquad (2\text{-}5)$$

where k is the harmonic number. For our application, the phase information of the fundamental component (k =1) is of interest. Therefore, the dielectric loss angle can be regarded as

$$\delta = \theta_v[1] + \pi/2 - \theta_i[1] \qquad (2\text{-}6)$$

Based on the RC combination representation and its phasor diagram (Fig 1.1), the capacitance of the apparatus can also be obtained by using the amplitudes of the fundamental components and the dielectric loss angle δ.

$$C = \frac{|X_i[1]|}{|X_v[1]| * 2\pi f} * \cos(\delta) \qquad (2\text{-}7)$$

Where $X_v[1]$, $X_i[1]$ and $\theta_v[1]$, $\theta_i[1]$ are the amplitudes and initial phases of the voltage and current signals respectively.

2.2 Measurement System

As shown in Fig. 2.2, the developed digital system is composed of a data acquisition circuit and software support components developed using Labview. The analog signals are scaled down by devices such as dividers and shunt resistors. The National Instruments NI-5102 Digital Storage Oscilloscope (DSO) board implements sampling of the analog voltage and current signals from the test object. The DSO board has channels which sample simultaneously; this eliminates the necessity of calibration to account for the time difference due to non-simultaneous sampling. The maximum real-time sampling rate is 20MS/s providing the possibility to study the effect of high sampling rate on the measurement results. Moreover, due to the large on-board memory and fast speed of data transfer to the CPU, the processing time is also reduced.

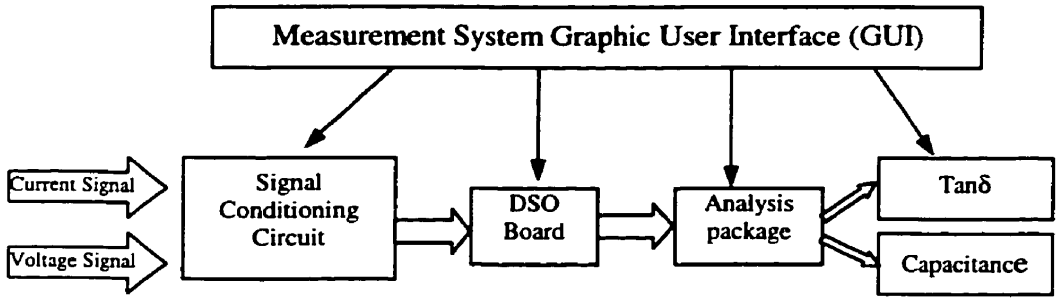

Figure 2.2 Schematic diagram of measurement system

The National Instruments software Labview is a general-purpose programming system based on the graphic language G. It creates programs, called Visual Instruments (VIs) since their appearance and operation can imitate actual instruments, in block diagram form. Labview is specially designed for engineers and scientists to provide

solutions for data acquisition, data analysis, data presentation and data storage. In our system, Labview is widely used to provide support for communication between the DSO and CPU, develop an analysis package for the digital computation of tanδ and capacitance, and build the graphic user interface (GUI). Fig 2.3 shows this graphic user interface (GUI) of the system, which consists of many adjustable parameters to control the measurement (see Appendix A).

Labview is also an open system, and algorithms built using other environments can be added through the form of Dynamic Link Library (DLL), which is helpful for future expansion of the developed digital system.

Figure 2.3 Measurement system graphic user interface (GUI)

2.3 Computer Software Simulation

When performing the DFT on the sampled data, the lack of synchronization between sampling rate and signal period is believed to be the main source of error in the measurement of the magnitude and the phase of the signal [12]. Due to the limitation of the time base of the DSO board (0.05μs) and power system frequency, asynchronization exists in the measurement system. Therefore, a software simulator was built to find errors caused and optimize performance of the developed system.

In the simulation, voltage and current signals were digitally generated with known phase difference, (90-δ), and accordingly known dissipation factor value. The digital generation emulated the function of the DSO board in the creation of the signals, and the DFT method was applied to calculate the dissipation factor, which was compared to the known value.

The simulated values of dissipation factor were chosen to lie in the realistic and practical range of 0.1% to 2%. The above technique was used to investigate errors associated with the sampling rate, voltage harmonics, frequency fluctuation and effect of choice of trigger point location. The simulation results show that errors in dissipation factor are found to be independent of the value of simulated dissipation factor, although the effects of these factors are different as discussed in the following section.

2.3.1 Sampling Rate

With a higher sampling rate the number of sampled data will increase and the resemblance between sampled data and actual signals becomes better. In the simulation

sampling rates chosen were those that could be obtained using the DSO board with a time base of 0.05μs, and the results are shown in Fig. 2.4. It can be seen that the error decreases with increase in the sampling rate but saturates after the sampling rate reaches a certain value. This saturation may mainly be due to the limitation of the vertical sensitivity of the DSO board. However, a disadvantage of employing a high sampling rate is that more data have to be processed resulting in longer processing time.

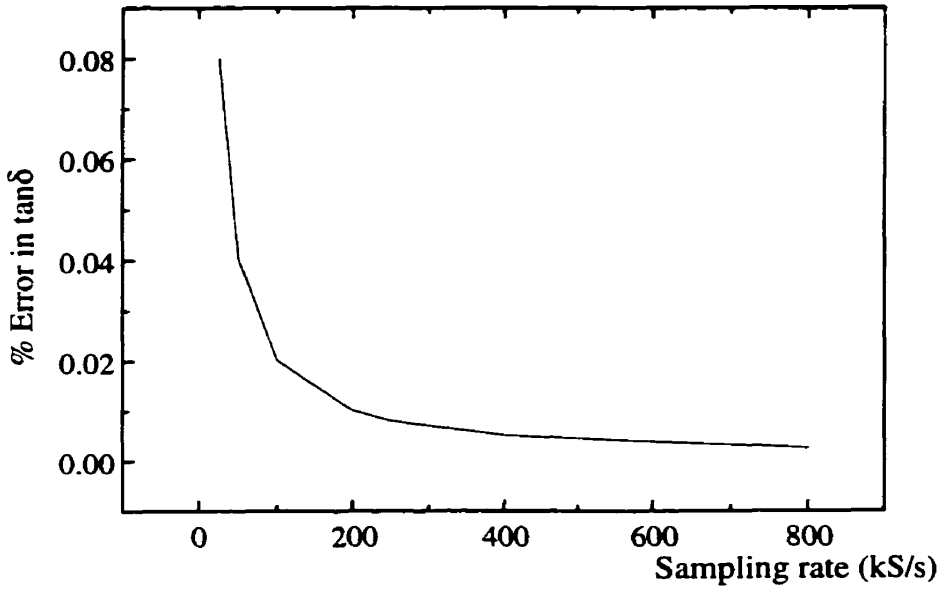

Figure 2.4 Relationship between sampling rate and measurement error

2.3.2 Effect of Harmonics

The signals in a power system are usually harmonic contaminated. The existence of harmonics causes significant error in the method of zero detection. Usually, the third and fifth harmonics are dominant. Table 2.1 shows typical data of the harmonic components in the High Voltage laboratory, University of Manitoba [13].

Table 2.1 Harmonic content in 120V laboratory power source

Time	Ratio to fundamental of			
	3rd harmonics	5th harmonics	7th harmonics	9th harmonics
Jan 7, 16:17	1.14%	1.50%	0.40%	0.33%
March 1, 18:07	1.82%	1.77%	1.19%	0.19%
April 10, 17:36	1.29%	1.78%	0.85%	0.30%
August 22, 17:25	2.13%	1.41%	0.40%	0.30%

Harmonic components of simulated voltage signals were chosen according to the data in Table 2.1. As to those of the digitally generated current signal, the ratio was calculated based on Eq. 2.8. where k is harmonic number, $\omega = 2\pi f$ is the angular frequency and the power frequency, f, is equal to 60Hz. Typical voltage and current waveforms employed in the simulation are shown in Figs. 2.5 and 2.6 respectively.

$$I_k = j * k * \omega * C * V_k \tag{2-8}$$

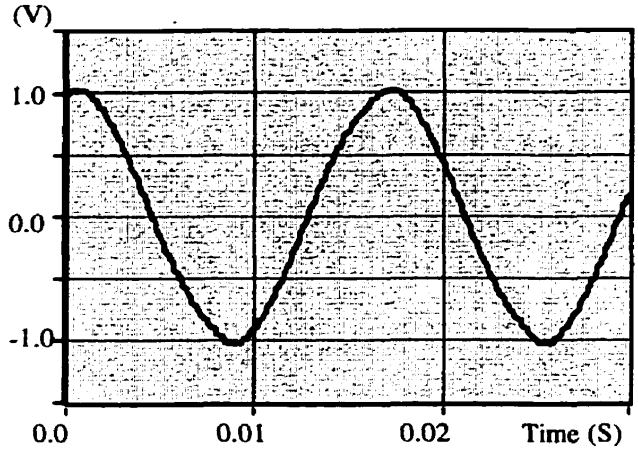

Figure 2.5 Typical simulated voltage signal

(Harmonic content: 3rd: 2.13%; 5th: 1.41%; 7th: 0.40%; 9th: 0.30%)

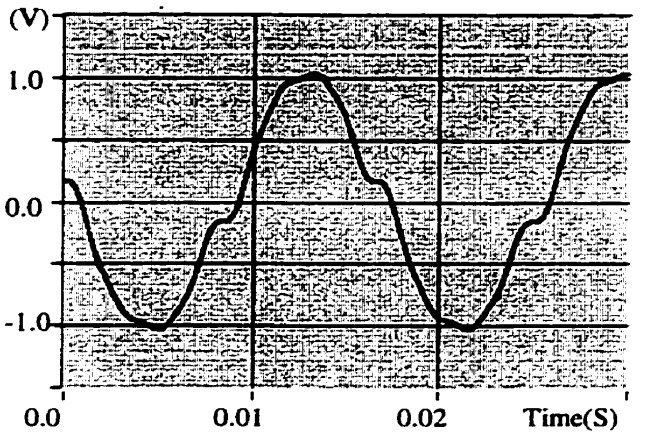

Figure 2.6 Typical Simulated current signal

(Harmonic content: 3rd: 6.39%; 5th: 7.05%; 7th: 2.80%; 9th: 2.70%)

As shown in Fig. 2.7, the results indicate that the error due to the existence of harmonics decreases with increase in the sampling rate. In addition, errors are negligible after a certain sampling rate. It proves that the proposed digital method is advantageous in effectively eliminating the influence of harmonics.

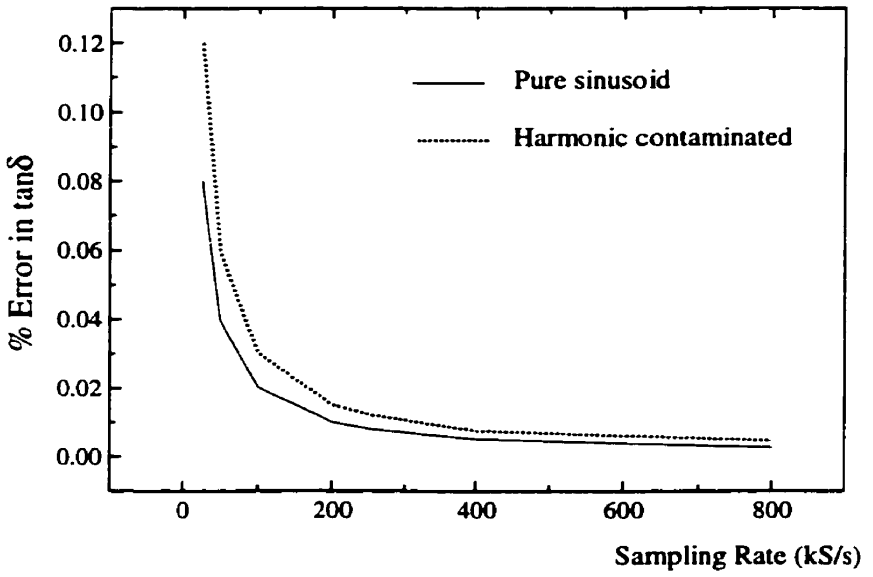

Figure 2.7 Effects of harmonics on tanδ values

2.3.3 System Frequency Fluctuation

In the measurement, the frequency in a power system is assumed to be exactly 60Hz. However, in practice, the system frequency always fluctuates to some extent (±0.05Hz). This will affect the measurement results since it causes asynchronization. To find the effects of the frequency fluctuation, the simulation over a wide range of frequencies were performed and the results are shown in Fig. 2.8.

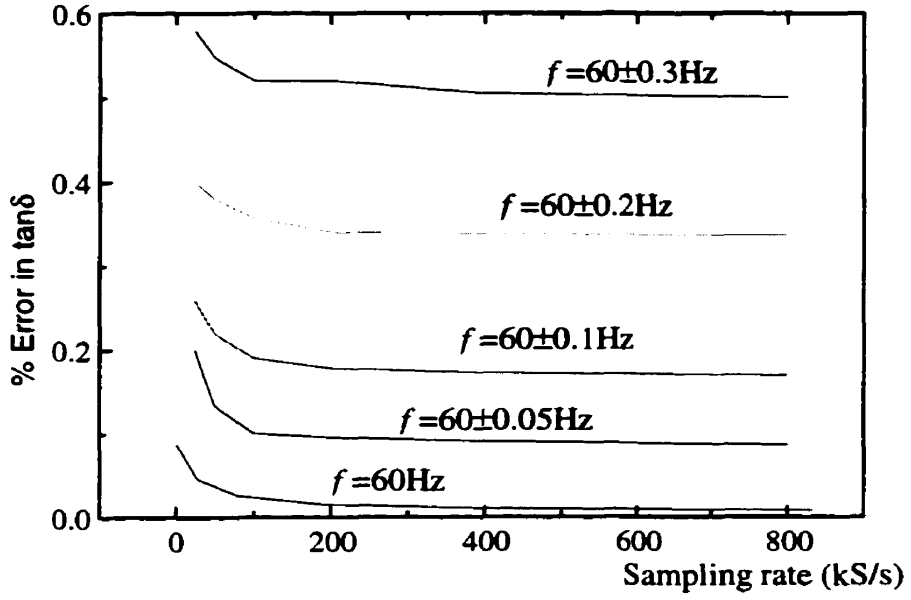

Figure 2.8 Effect of system frequency fluctuation

2.3.4 Trigger Points

The effect of choice of trigger point location was also studied. In the software simulation, the simulated voltage signals are chosen as the reference and data sampling started at a chosen location on the voltage reference waveform, called the trigger point. The illustration of trigger point selection is shown in Fig. 2.9. Independent of the trigger

point locations, the sampling of the current signal starts simultaneously with that of the voltage signal.

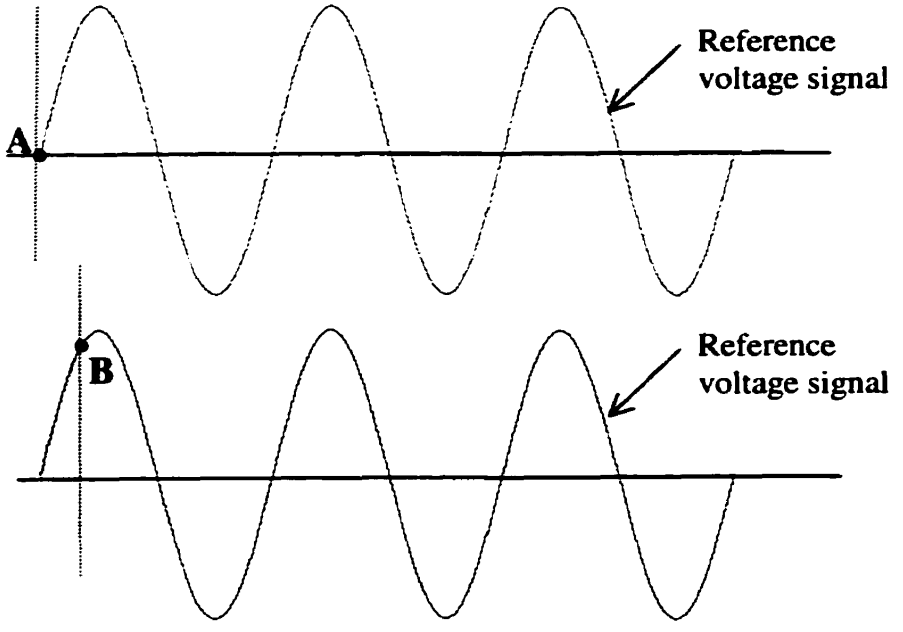

Figure 2.9 Illustration of trigger point selection

Top waveform: Sampling starts at point A on reference voltage signal
Bottom waveform: Sampling starts at point B on reference voltage signal

Fig. 2.10 shows a typical error trend dependent on the choice of trigger point locations on the voltage waveform. The error variation is seen to be cyclic independent of the change of sampling rate, frequency fluctuation and voltage harmonics. Accordingly, if a number of measurements are made with trigger points located in the range between 0 and 360 degrees, then the average will have zero error. In addition, the error indicates that the errors can be minimized by choosing some specific trigger points such as 0, 90, 180, 270 and 360 degrees. As a matter of fact, both the above techniques were used in the laboratory and on-site tests.

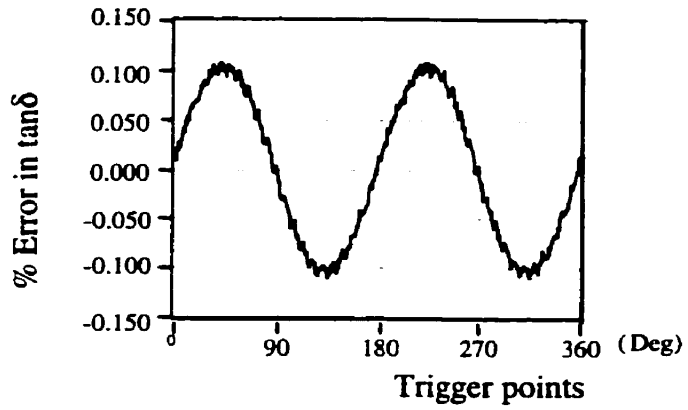

Figure 2.10 Effect of trigger points
(Sampling rate =25kS/s)

2.4 Laboratory Tests

Laboratory tests were carried out in order to evaluate the system performance and find optimal measurement parameters. In this procedure, tests were conducted in two stages. First, the tanδ and capacitance of a low-loss capacitor were measured under low voltage. In addition, the effects of sampling rate, trigger point location and the number of sampled cycles on the measured values of tanδ were investigated. In the second stage, the tanδ and capacitance of a 40kV, 500pF power capacitor were examined under high voltage.

2.4.1 Low Voltage Tests

2.4.1.1 Set-up

The tests were performed to verify the developed system and the set-up is shown in Fig. 2.11. Dielectric loss was simulated using a combination of a metal film resistor R_c

(low inductance) and a low loss polystyrene capacitor C_e. A wide range of tanδ values were simulated by varying the values of R_e and C_e.

Power was supplied from a wall-outlet through a variac (0-110V output voltage, 1kVA). The voltage signal was derived from a resistive divider (R_1 &R_2), while the current signal was obtained from the voltage drop across the resistive shunt R_s. Both signals were conveyed to the developed system for analysis. Errors introduced are mainly due to the insertion of shunt resistors and the conditioning circuit, which were calibrated by software calculation.

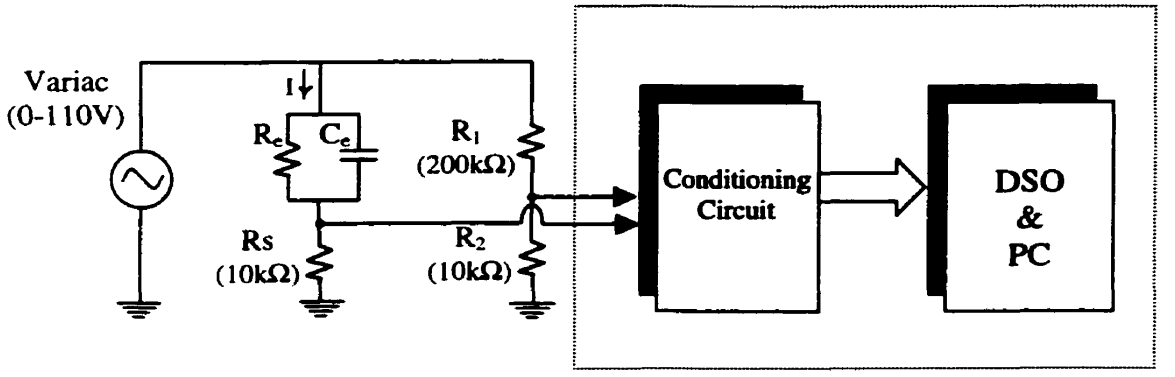

Figure 2.11 Set-up in the low voltage tests

2.4.1.2 Test Results

In the tests, no two measurements are identical and the results display a statistical feature. Typical results are shown in Fig. 2.12, which were obtained with a sampling rate of 25kS/s, random trigger point locations and data acquisition over one cycle. It indicates that a significant error of 0.25% exists in the tanδ measurement.

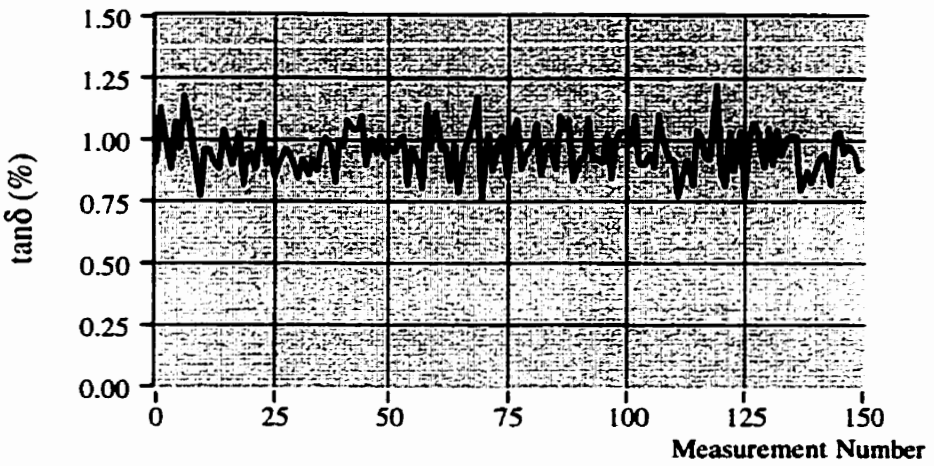

Figure 2.12 Typical results of measurement; calculated tanδ =0.935%

(25kS/s sampling rate, random trigger points, data acquisition over one cycle)

By increasing the sampling rate, the results indicate that a significant improvement results in measurement accuracy. Moreover, the sampling rate has the effect similar to that obtained by software computer simulation: the influence of sampling rate is significant at first while the error becomes negligible after the sampling rate reaches 200kS/s. Further increase in the sampling rate only leads to increased processing time. Typical test results obtained at different sampling rates are shown in Fig. 2.13.

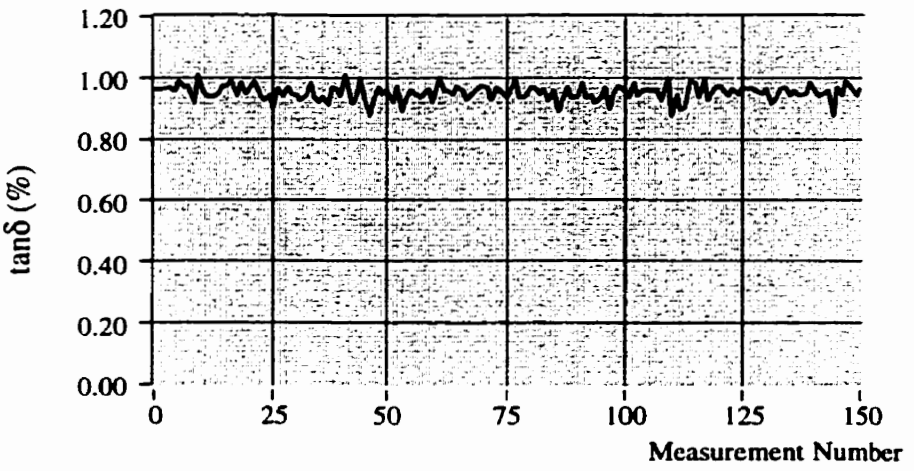

(a) Sampling rate = 200kS/s

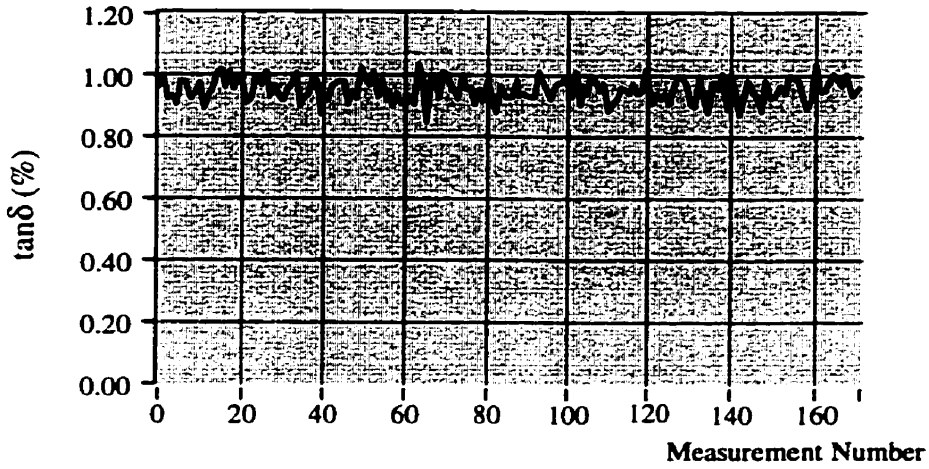

(b) Sampling rate = 400kS/s

Figure 2.13 Effects of sampling rate in the low voltage tests
(random trigger points, data acquisition over one cycle , calculated tanδ = 0.935%)

The measurement accuracy and stability can be also improved by controlling trigger point location and the number of sampled cycles. Trigger level was set based on the fundamental quantity and the start angle of the voltage signal. In the tests, it was found that the 10-cycle average value of tanδ was optimal in the sense that the error reaches a stable minimum value and the processing time is not too long. With further increase of the number of sampled cycles, the processing time increases without any significant gain in accuracy. Fig 2.14 shows the results obtained with a 25kS/s sampling rate and trigger point located at zero degree. Each measurement point represents the average of tanδ computed over 10 cycles. Comparing with Fig 2.12, the significant effects of trigger point locations and the number of sampled cycles are obvious.

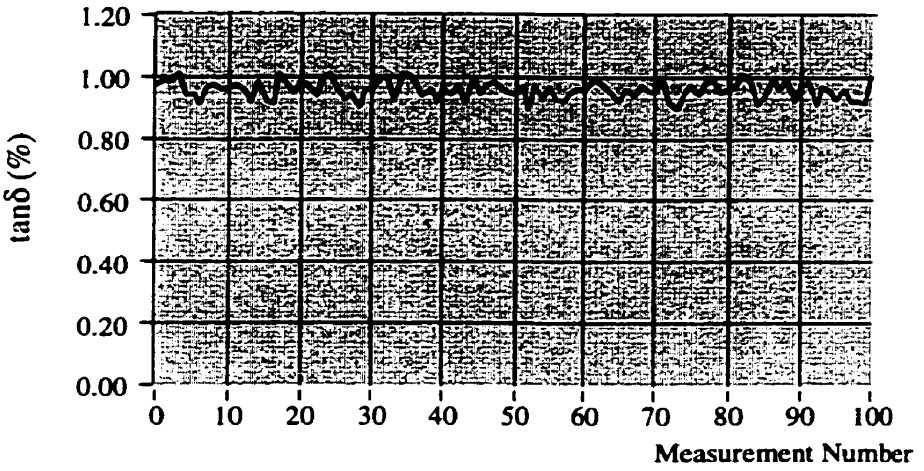

Figure 2.14 Illustration showing the effects
of trigger point locations and number of sampled cycles
(25kS/s sampling rate, trigger point = 0^0, data acquisition over 10 cycles)

By comparing the results obtained with different measurement parameters, the optimal measurement parameters are: 200kS/s sampling rate, trigger point located at zero degrees, and data acquisition carried out over 10 sample cycles. A typical trend of the results obtained with the optimal parameters is shown in Fig. 2.15.

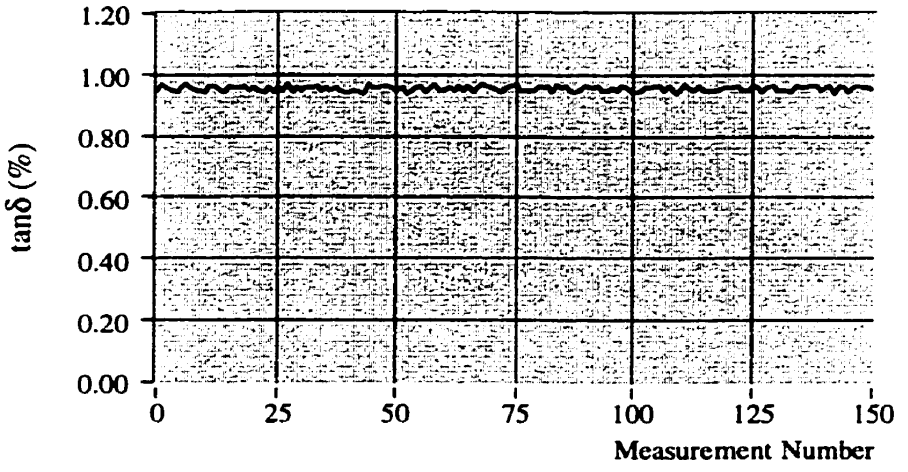

Figure 2.15 Results obtained with optimal measurement parameters
(calculated tanδ =0.9348%)

The tanδ values were also calculated from known values of R_e and C_e in order to make a comparison with that obtained from tests. Table 2.2 shows the comparison of the calculated values and test values with the optimal measurement parameters. In the calculation, the capacitor C_e is assumed to be lossless.

Table 2.2 : Comparison of calculated values and test values with optimal measurement parameters

R_e (MΩ)	C_e (PF)	Calculated tanδ (%)	Measured tanδ (%)	Measurement Precision
∞	4400	0	0.032	± 0.04%
129.1	4400	0.467	0.491	± 0.05%
64.5	4400	0.935	0.965	± 0.05%
33.0	4400	1.827	1.849	± 0.04%

2.4.2 High Voltage Tests

2.4.2.1 Set-up

Fig. 2.16 shows the measurement set-up under high voltage. A 40kV, 500pF power capacitor was chosen as the test sample. To measure tanδ and capacitance, the voltage signal was obtained using a capacitive divider composed of low-loss capacitors, while the current signal was derived from the voltage drop across a resistive shunt. In the tests, the peak value of the applied high voltage was 15kV.

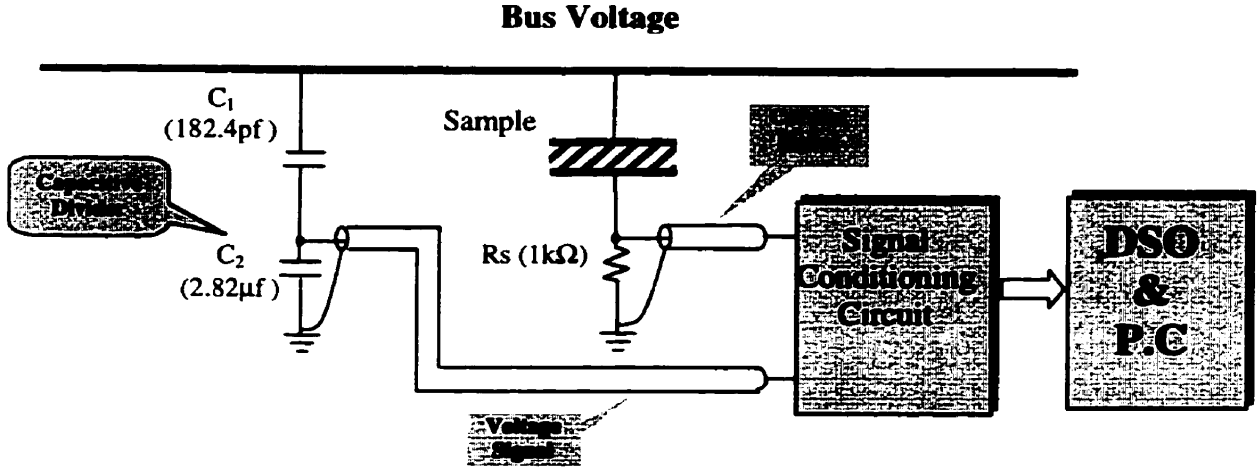

Figure 2.16 Set-up in the high voltage tests

2.4.2.2 Test Results

Tests were carried out with the measurement parameters chosen at optimal values (section 2.4.1) found in the low voltage tests. Phase shifts introduced are mainly due to the introduction of capacitive divider and the conditioning circuit, which were calibrated by software calculation. A typical trend of results is shown in Fig. 2.17. To evaluate the results obtained, the measurement of dissipation factor and capacitance was also performed by use of a HAEFELY current comparator, which has an accuracy of 1×10^{-5} in $\tan\delta$ measurement. Both results are shown in Table 2.3. The comparison indicates that the measurement precision of the developed digital method is limited to ±0.05% for the values of $\tan\delta$, while the relative error in the capacitance measurement is 0.2%. In addition, it was found that there was no change in the measured results obtained using the developed system when the conditioning circuit was omitted in the set-up (Fig 2.16).

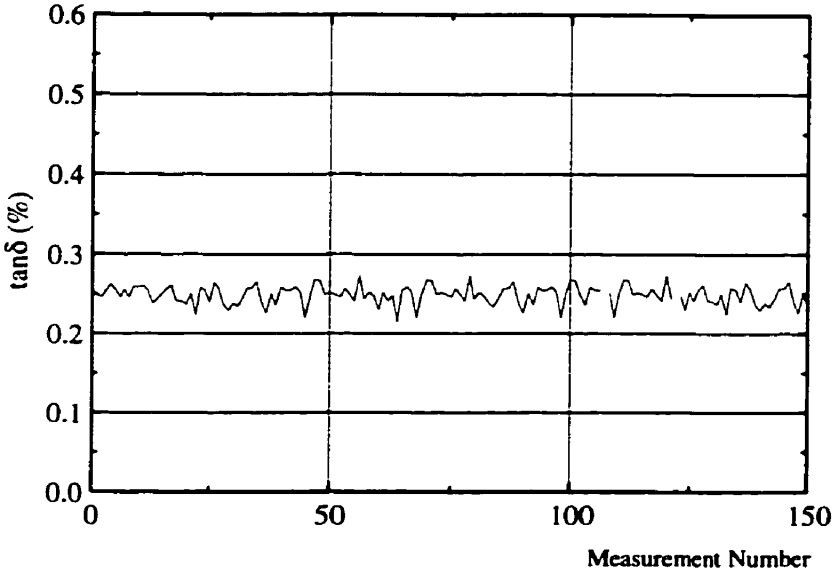

Figure 2.17 Typical tanδ values in the high voltage tests
(200kS/s, trigger point =at 0°, average of 10 cycles)

Table 2.3 Comparison of the measured results with optimal parameters

Results			Test Voltage			
			2.5kV	5kV	10kV	15kV
Tanδ (%)	HAEFELY current comparator		0.239	0.235	0.236	0.267
	Developed System	Values	0.217	0.204	0.221	0.248
		precision	±0.04%	±0.05%	±0.05%	±0.04%
C (PF)	HAEFELY current comparator		520.14	520.17	520.18	520.48
	Developed System		520.68	520.78	521.10	521.34

2.5 Method Employing Cancellation of Capacitive Current

2.5.1 Principle

The dielectric loss angle of high voltage apparatus is usually very small except under conditions of significant insulation deterioration. For apparatus with large capacitance, tanδ will become even smaller for the same loss. Therefore, for specimens of high capacitance a higher sensitivity in the measurement is called for. This may be achieved by partial cancellation of the high capacitive current by means of a generated capacitive current of opposite sign. In this manner, the dielectric loss angle can be artificially increased. The phasor diagram of the method is shown in Fig. 2.18.

In Fig. 2.18, I_{Re} and I_{ce} represent the original resistive and capacitive currents through the test sample respectively, and the total current is I_1. By generating the cancellation capacitive current, I_c, the capacitive current component is reduced and becomes $(I_{ce}-I_c)$, the reduced capacitive current. Accordingly, the dielectric loss measured becomes $\tan\delta_2$, which is larger and easier to measure. The real dielectric loss $\tan\delta_1$ can be obtained after correction for introduction of the cancellation capacitive current.

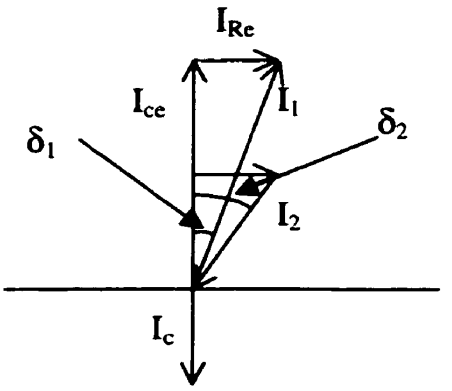

Figure 2.18 Phasor Diagram of the method employing cancellation of capacitive current

2.5.2 Computer simulation

Computer simulation was carried out to find the effects of voltage harmonics, ratio of the reduced capacitive current to the original capacitive current (cancellation current ratio), and sampling rate. If signals are harmonic free, the error is found to increase with the cancellation current ratio. Other parameters have effects similar to those discussed in section 2.3.

However, if the signals are harmonic contaminated, the situation becomes complex. In this case, the location of the trigger point has a similar effect, but the curve (Fig 2.10) shifts with change in the cancellation current ratio. In contrast with the results shown in Fig.2.10, the error in the average value of several measurements, conducted with trigger points located in the range between 0 and 360 degrees, is not equal to zero. Also, the errors in tanδ are dependent on the actual values of tanδ. This is not the case when the cancellation technique was not employed. Fig. 2.19 shows the simulation results for harmonic contaminated signals.

2.5.3 Laboratory low voltage tests

The measurement set-up is shown in Fig. 2.20. A sinusoidal waveform generator was used as the power supply, which can provide adjustable output voltage between 0 and 25V(RMS). To measure tanδ and capacitance, the voltage and current signals were derived from the circuit in the same manner as that discussed in section 2.4.1. Besides, the metal film resistor R_4 is adjustable to control the output voltage of the inverting circuit.

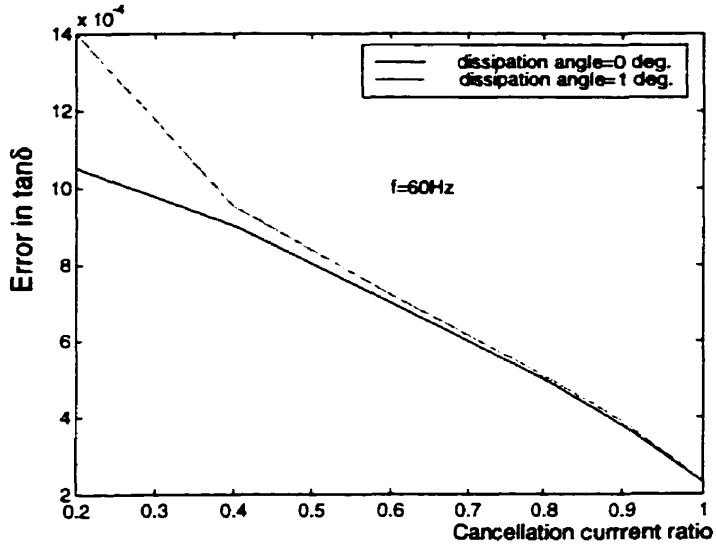

Figure 2.19 Simulation results for harmonics contaminated signals

Two types of tests were conducted which differed in the manner in which the cancellation capacitive current was generated. In one method, the cancellation capacitive current was software-generated by shifting and scaling of the voltage signal, while an inverting circuit and low-loss polystyrene reference capacitor C_I (Fig. 2.20) was

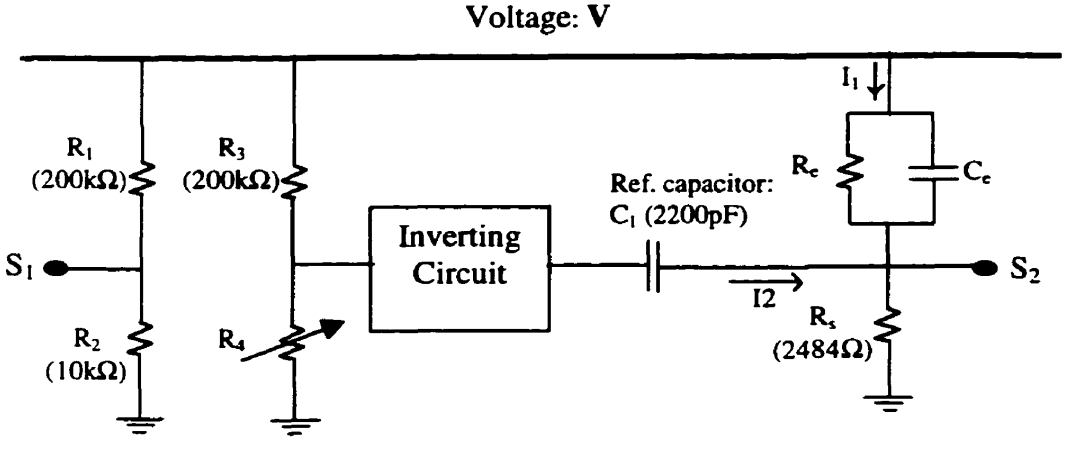

Figure 2.20 Set-up for the method of canceling capacitive current

S_1: Voltage signal S_2: Current signal

employed to hardware-generate the cancellation capacitive current in the other method. The results are shown in Fig. 2.21.

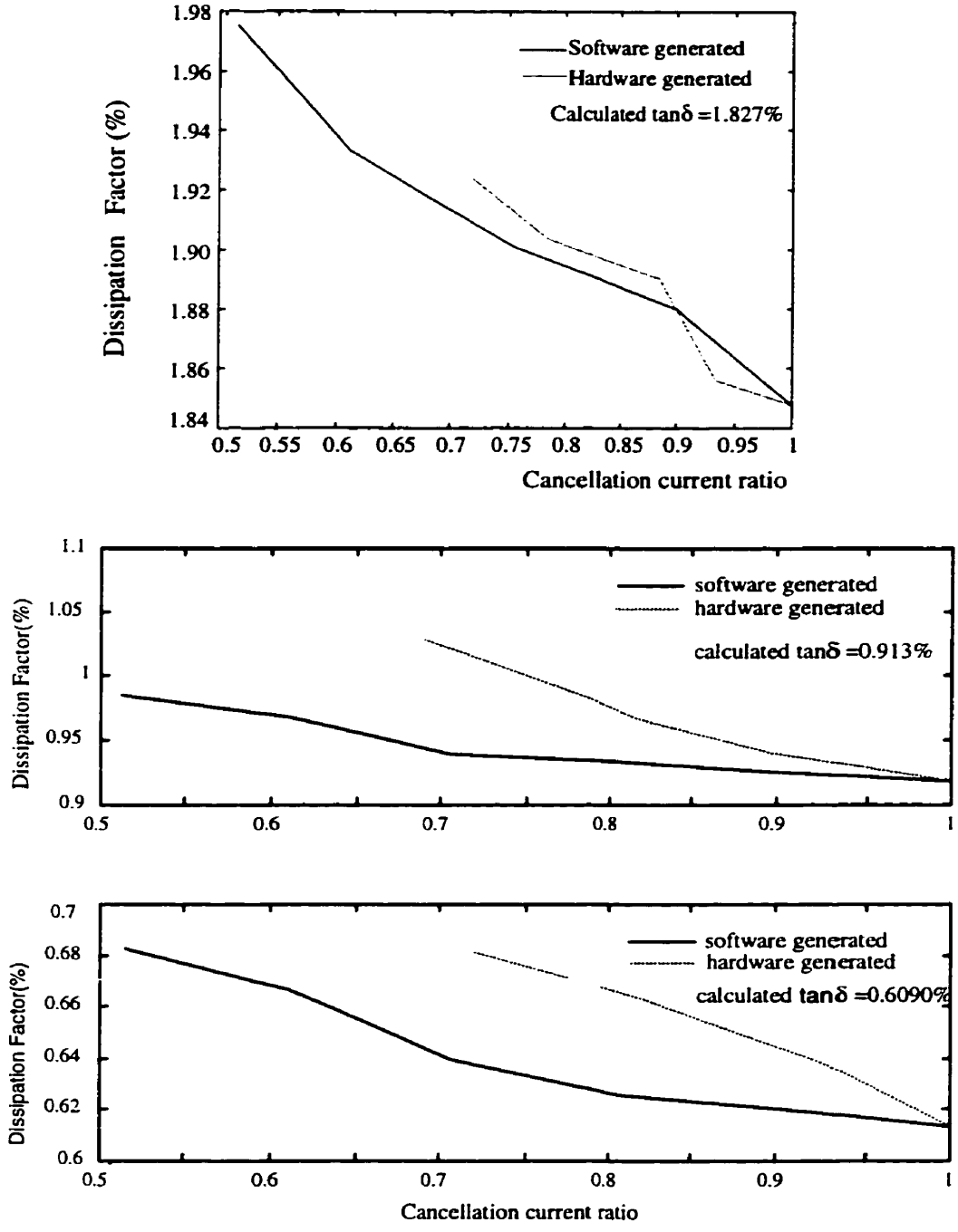

Figure 2.21 Test results using the cancellation of capacitive current

From Fig 2.21, it can be seen that errors in both methods increase with decrease in the cancellation current ratio. Also, this trend is the same as that obtained by using computer simulation as discussed in section 2.5.2. In the tests, there are two reasons which account for the observed errors. If the cancellation capacitive current is software generated, it is not possible to achieve exactly a 90-degree shift of the voltage signal. Insertion of the inverting circuit and the effects of voltage harmonics account for the errors in the method which employs hardware–generation of the cancellation capacitive current. The results also indicate that the cancellation technique has acceptable engineering accuracy.

CHAPTER 3

ON-LINE MEASUREMENT OF DISSIPATION FACTOR AND CAPACITANCE OF HIGH VOLTAGE INSULATION

Dissipation factor (tanδ) and capacitance are two key parameters that define the insulation condition of high voltage apparatus. Generally, these values depend on the operating voltage, temperature, and insulation condition, in addition to the design, materials used and production technology. Capacitance and tanδ can be advantageously obtained using an on-line digital method due to the fact that no service interruption is required thus resulting in low labor cost. Moreover, on-line measurements under operating voltage can be more helpful to reflect the real status of insulation and to detect defects.

To implement a digital method, a reference signal is necessary to provide the basic phase information. If a standard gas capacitor is used to provide the reference, the measured values may be regarded as being absolute since the dielectric loss angle of the standard capacitor is almost "zero". If the reference is obtained by using other unit, the measured tanδ values are relative with respect to the insulation of that unit. However, tanδ is, by nature, a relatively slowly changing value; thus the trend of values with respect to time gives important information about the insulation property even if the measured value is not absolute.

In this work, a system for on-line monitoring of tanδ and capacitance has been developed based on the digital method, which is discussed in chapter 2. The scaled down signals are acquired using a Digital Storage Oscilloscope (DSO) board, while the graphic user interface and the analysis package are implemented with G language software Labview. The field tests were conducted at Manitoba Hydro's Dorsey station to evaluate the insulation of a current transformer (CT) unit, which is located on the 230kV line from Dorsey to St. Leon shown in Fig. 3.1.

Figure 3.1 CT unit and measurement system layout

3.1 Test set-up for on-line measurement

Fig. 3.2 shows the basic measurement set-up. The insulation of the CT unit is regarded as a RC combination. Two signals are acquired in the circuit, a reference voltage signal from the voltage transformer (PT) and a current signal from the test object.

3.1.1 Voltage signal

The secondary side (69V) of the voltage transformer was used to provide the reference signal. The voltage transformer has an accuracy class of 0.3WXY for the 2000:1 ratio. To scale down this reference signal a voltage conditioning circuit (Fig. 3-2-a) was built, and it was connected to the PT using a 900 foot long control cable (United Wire & Cables Inc). In the voltage conditioning circuit, all resistors are of the metal film type to eliminate the inherent

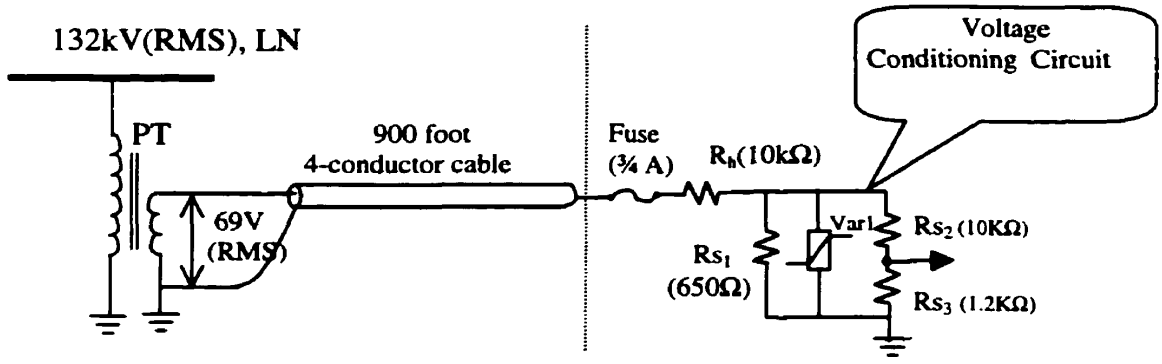

(a) Measurement set-up for voltage signal (single phase)

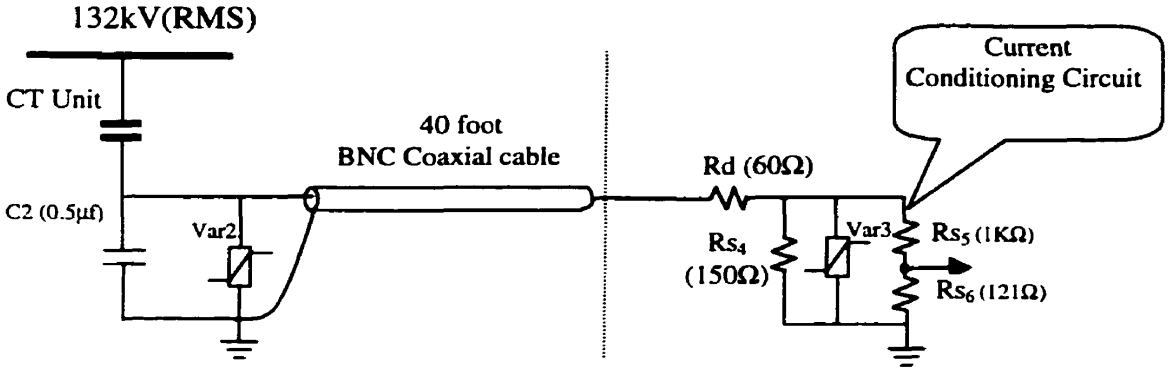

(b) Measurement set-up for current signal (single phase)

Figure 3.2 Test set-up for on-line measurement

inductance. A Siemens disc type metal oxide varistor Var1 with clamping voltage of 36V was connected to provide transient overvoltage protection. In order to protect against an accidental short circuit, a fuse rated ¾ ampere was put into the circuit.

3.1.2 Current signal

Generally, two methods are employed to obtain the current signal from the test object: a combination of a resistive shunt and a bypass switch, or current sensors such as Rogowski coil. The former method is simple and reliable, but does not ensure safe operation. Due to significant electromagnetic interference in the field and the weakness of the input signal, the current sensor signal should be stable and reliable.

In our system, the current signal is derived from the voltage across the combination of a ceramic capacitor C2 and the current conditioning circuit (Fig. 3-2-b). The ceramic capacitor C2 is included to provide a safe low voltage connection, and the current conditioning circuit functions as a resistive shunt with transient protection feature. A metal film resistor Rd was employed to damp overvoltages which may occur due to stray inductance in the circuit (discussed in section 3.2). The transient protection device consists of two parts: varistor Var2 and varistor Var3. The rated voltage of the Harris varistor Var2 is 420V which can limit the possible overvoltage applied at the front end of the cable, while varistor Var3 is of the same type as Var1 and has a clamping voltage of 36V.

3.2 System hardening

Both current signals and voltage signals have to be acquired using the DSO board before the digital computation of tanδ and capacitance. Due to the input voltage limitation of the DSO board (maximum transient voltage 40V), the measurement system was hardened to protect it from the damaging effect of transient overvoltages. This function was implemented by using the conditioning circuit, a combination of a Seimens varistor, resistive shunts and dividers (Fig. 3-2). In order to verify the transient protection characteristics of the conditioning circuit, laboratory tests were carried out using the set-up shown in Fig. 3.3.

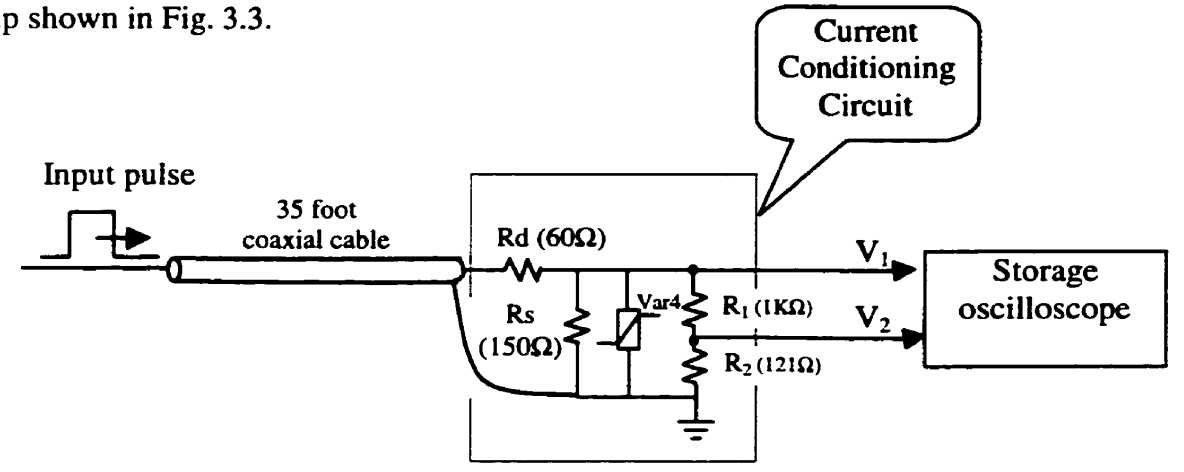

Figure 3.3 Assessment of transient performance of the current signal circuit

A Noise Laboratory Co. Ltd pulse generator (2 nanosecond rise time, maximum 2000V) provided the input pulse, which is shown in Fig. 3.4. The varistor Var4 is of the same type as varistors Var1 and Var3, and the ratio of resistive divider (R_1 &R_2) was set to be 1000/121 (Fig. 3.2). The maximum input pulse magnitude was chosen to be 1000V, and two output voltages were recorded using a Textronix TDS320 oscilloscope

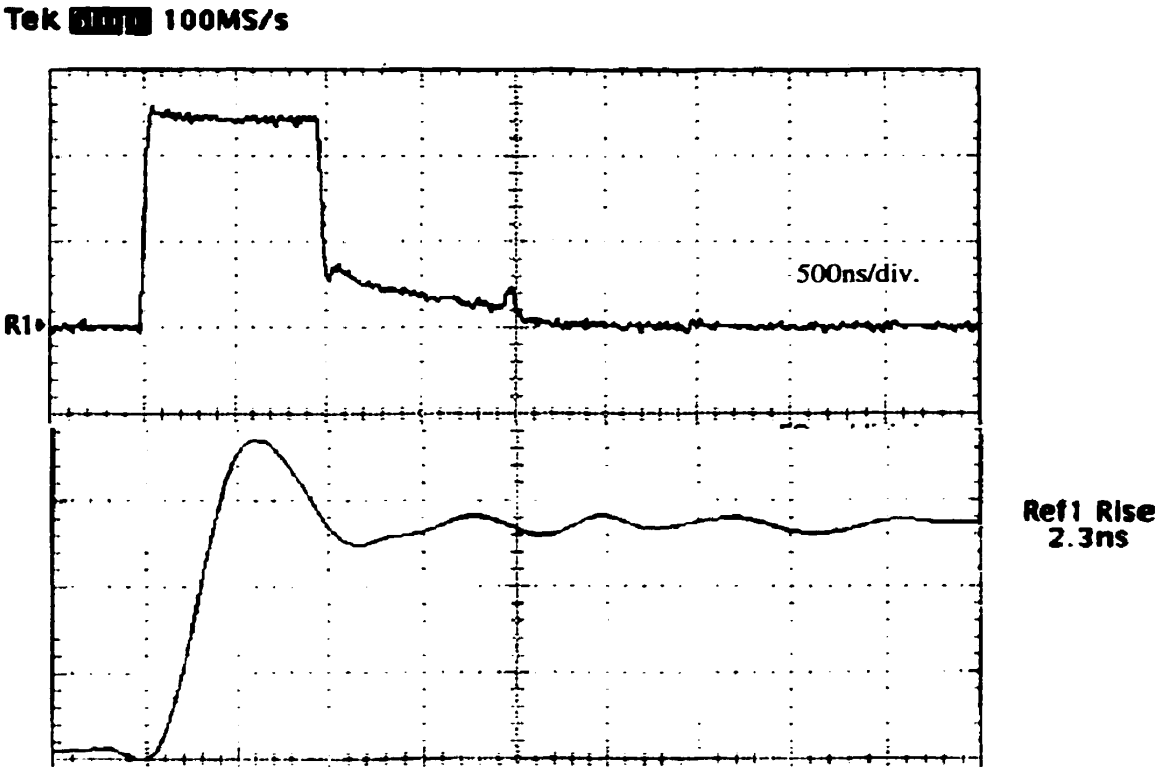

Figure 3.4 Input pulse provided by the pulse generator

i.e., V_1, the voltage across the varistor Var4 and V_2, the voltage applied to the DSO board. Initially the damping resistor, R_d, was not employed in the circuit. Due to stray inductance in the circuit, the protection device did not work efficiently. Therefore, the damping resistor, R_d, was introduced in the circuit. Fig. 3.5 shows the output voltage with 1000V input pulse when damping resistors of 30, 60 and 120Ω were included. Each figure consists of the recorded voltage V_1 (top) and Voltage V_2 (below). The result indicates that output voltage V_2 will be 4.3 volts with 1000V input for the 60Ω damping resistor. Therefore, if the ±5V input limitation of the DSO board is not to be exceeded the

maximum transient voltage at the end of the connected cable can not exceed 1160V. This translates to 800kV at the bus bar (Fig 3-2-a), which provides enough safety for the measurement system.

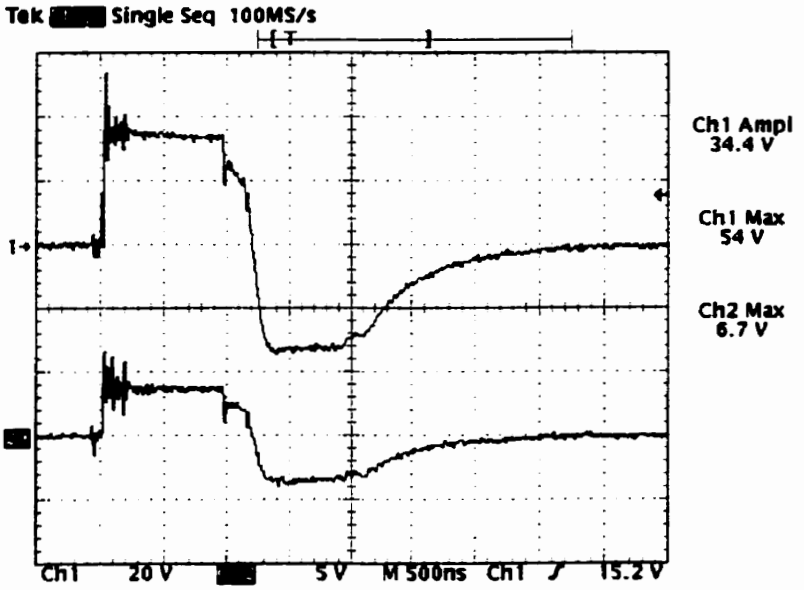

(a): 30Ω damped resistor

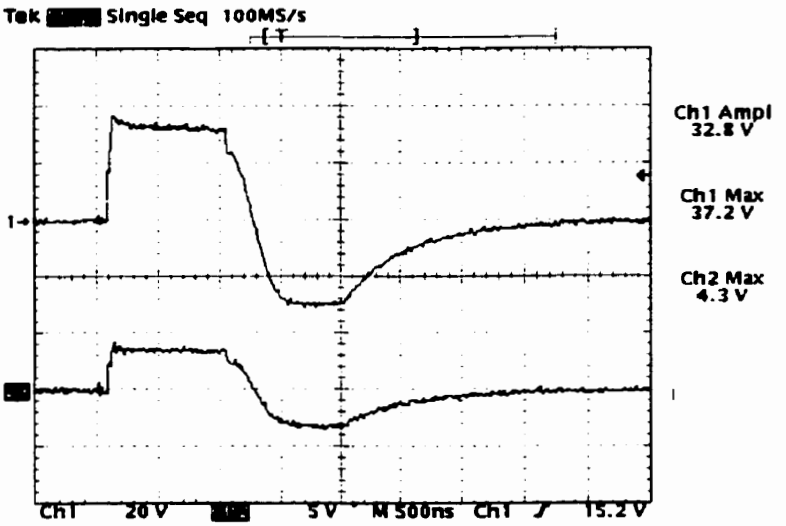

(b): 60Ω damped resistor

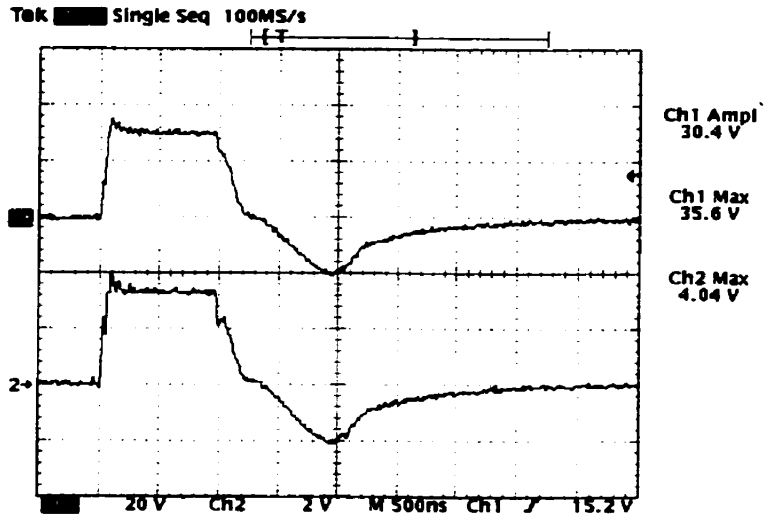

(c): 120Ω damped resistor

Top waveform: voltage across the varistor Var4 (V_1)
Bottom waveform: voltage applied to the DSO board (V_2)

Figure 3.5 Effect of the damping resistors on the output voltage

In the field tests, the CT unit, PT unit and power supply for the instruments are situated far away from each other. Due to possible ground currents, the ground potential for these units may be different and cause damage. Thus, two isolating transformers were used to separate the grounds and a common ground was produced. Fig 3.6 shows the connection configuration of measurement set-up.

3.3 Calibration

Measurement errors always exist due to the introduction of measurement components such as PT, the ceramic capacitor and cables. In order to obtain accurate results, these errors must be corrected by performing corresponding calibration.

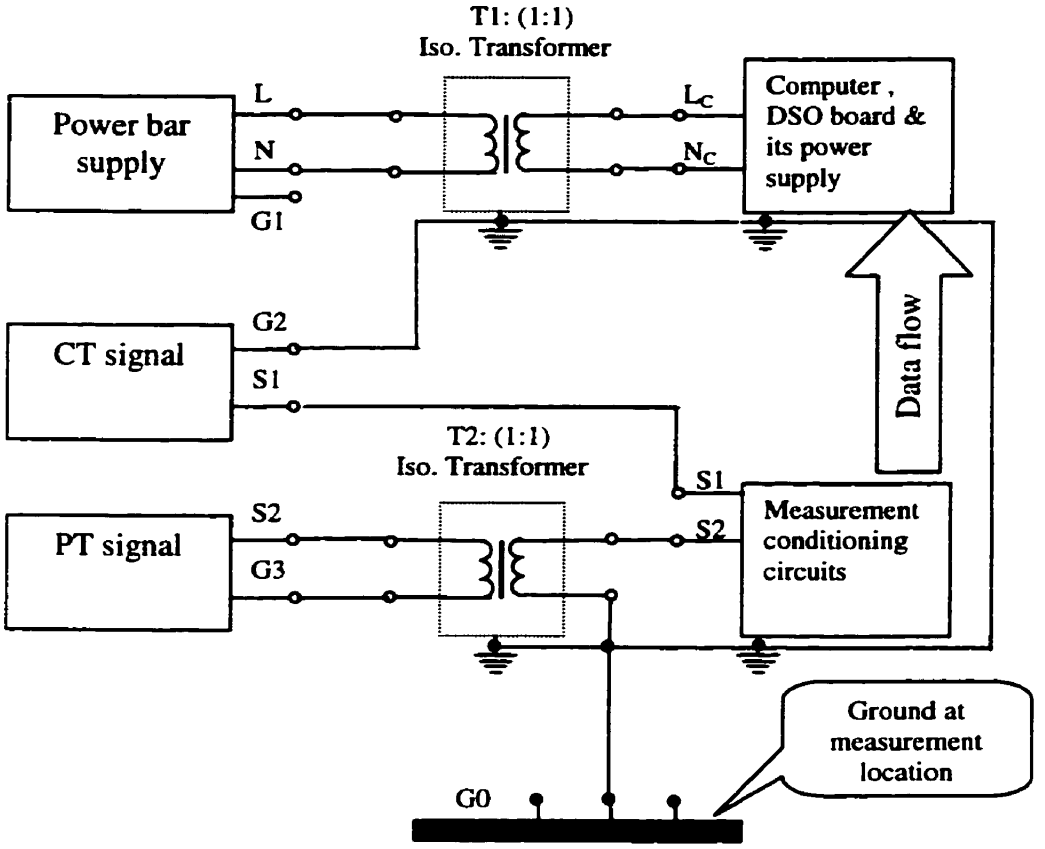

Figure 3.6 Connection configuration of measurement set-up

3.3.1 Calibration for the reference voltage signal

For the absolute measurement of tanδ, a standard gas capacitor should be included in the H.V. circuit to provide the reference signal. However, in the field tests, the signals are easier derived from the voltage transformer (PT). In our set-up, the PT was used (Fig. 3.7) so the phase shift between the primary and secondary voltage must be taken into account to get correct results.

Figure 3.7 Voltage transformer used for deriving voltage signal

3.3.1.1 Equivalent circuit of isolating transformer

To isolate ground current effects, a 1:1 ratio isolating transformer was used to connect the PT signal to the voltage conditioning circuit (Fig. 3-2-a), as shown in Fig. 3.6. This may cause phase shift and voltage ratio error. To evaluate the error, short circuit and open circuit tests were conducted on the isolating transformer to find its impedance. Next, voltage ratio tests were conducted to determine the exact voltage ratio. The equivalent circuit of the isolating transformer is shown in Fig. 3.8.

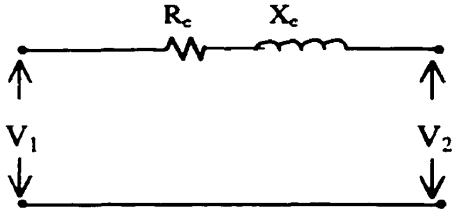

R_e=0.48 Ω
X_e=1.49 Ω;

O.C voltage ratio at rated voltage:
N=0.970

Figure 3.8 Equivalent circuit of the isolating transformer

3.3.1.2 Effect of connecting cable

A 4-conductor cable was used to provide the scaled down voltage signal from the PT to the measurement location, as shown in Fig. 3.9; this may have two effects. First it behaves as a burden of the PT. Second there could be inter-phase coupling. A cross-section of the cable and the measured values of the associated capacitance provided By Manitoba Hydro are shown in the Fig. 3.10. The measurement of tanδ was carried out in two ways. First only that phase was energized which was involved in the measurement. Next, the remaining two phases were energized as well but not used in the measurement. No difference was found in the results. This shows that inter-phase effects introduced by the 4-conductor cable are insignificant.

Fig. 3.9 4-conductor cable connected to the measurement location

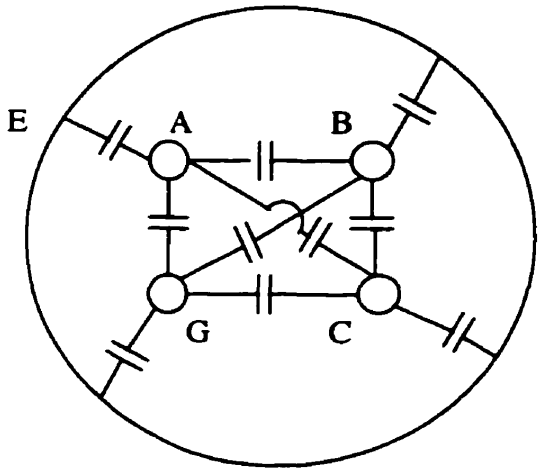

Per foot: C_{AE}=97.68pf
C_{BE}=80.67pf
C_{CE}=96.86pf
C_{GE}=82.63pf
C_{AB}=21.20pf
C_{BC}=21.54pf
C_{CA}=4.43pf
C_{AG}=22.80pf
C_{BG}=3.78pf
C_{CG}=23.68pf

Figure 3.10 Cross-section of the Cable and its associated Capacitance

3.3.1.3 Phase shift due to PT and its burden

The PT phase shift depends on its leakage impedance, the secondary burden, magnitude of applied voltage and harmonic component. Generally, the secondary burden has the most significant effect on the phase shift.

In the set-up, the 900-foot long cable, isolating transformer (Fig. 3.6) and the voltage conditioning circuit (Fig.3-2-a) essentially form the secondary burden. Fig. 3.11 shows the equivalent circuit for the calculation of the phase shift. The PT has a leakage impedance of 0.05Ω and the phase-ground capacitance of the cable was measured using the guarded capacitance bridge method. Based on the equivalent circuit, the phase shift due to the PT and its burden is 0.32% and is same for three phases (See Appendix B).

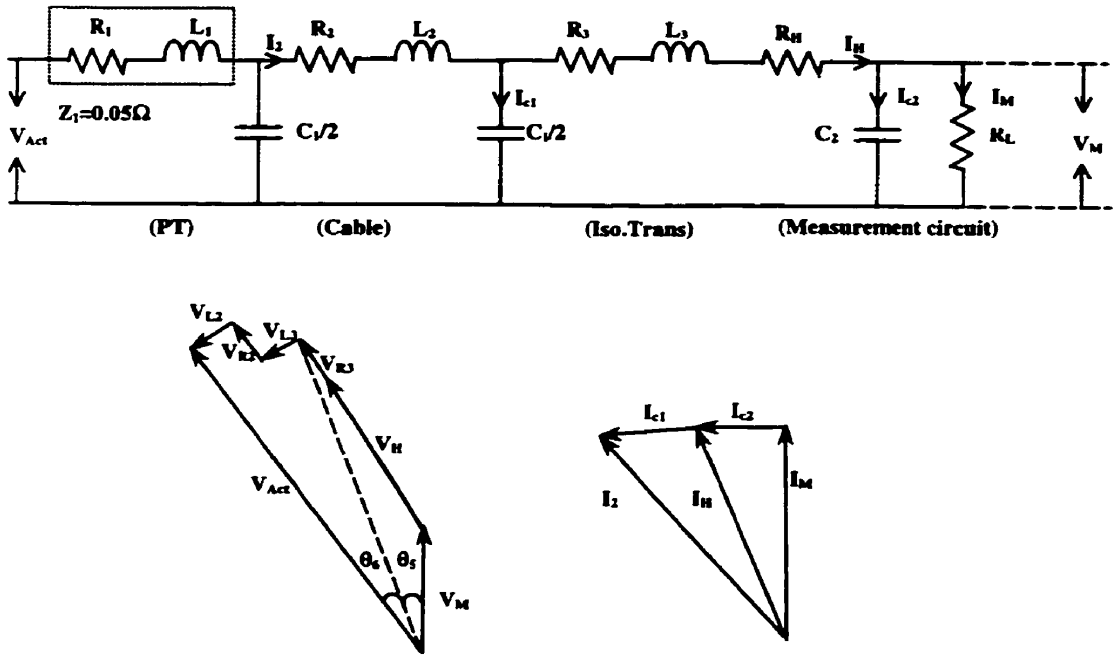

Fig 3.11 PT equivalent circuit for phase shift calibration

3.3.2 Calibration for the current signal

In the set-up (Fig. 3-2-b), the ceramic capacitor together with the insulation of the CT unit forms a capacitive divider, and this feature ensures safety. Also, this set-up can provide signals for other tests, such as partial discharge detection. However, the combination of the ceramic capacitor and current conditioning circuit introduces a phase shift. This phase shift depends on the resistance of shunts, capacitance of the ceramic capacitor and the ambient temperature because of the large temperature coefficient of the ceramic capacitor. An example of the effect of the temperature coefficient on the capacitance is shown in Fig 3.12. Thus, it is essential that the resistive shunt should be chosen properly to minimize the phase shift.

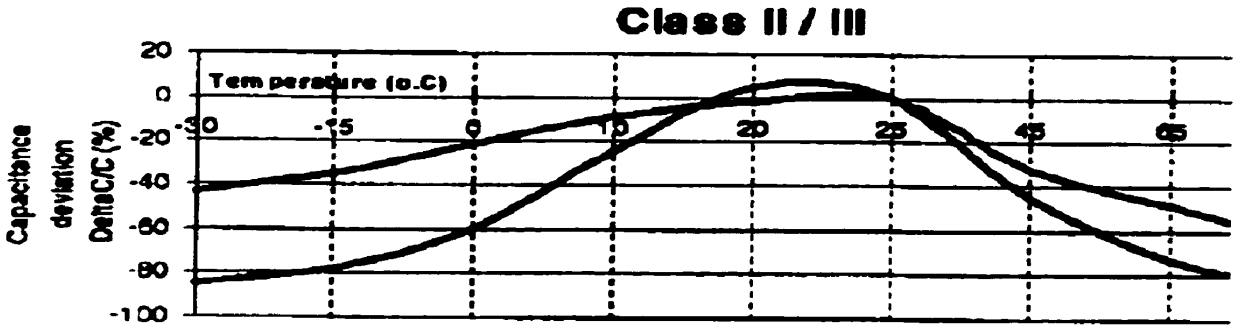

Figure 3.12 Effect of temperature coefficient on capacitance of the ceramic disc capacitor (AVX company) [www.avxcorp.com]

Since neither the exact value of the ceramic capacitor nor its temperature coefficient were known in our tests the following procedure was adopted in the measurement to account for the phase shift. First the voltage across the ceramic capacitor was recorded before connecting the conditioning circuit. Second, the measurement of tanδ and capacitance was carried out. Third, the capacitance of the ceramic capacitor was derived based on the measured CT capacitance using the voltage divider principle; the bus voltage was obtained from the PT readings. Finally, this derived value of the ceramic capacitor was used to calibrate the phase shift.

The above procedure is not an error free scheme. Measurement errors were introduced in the measurement of capacitance of the CT unit due to the fact that the ceramic capacitor drew some current even with very small shunt resistance. Also, the capacitance of the CT unit will change with temperature. However, the temperature coefficient of the ceramic capacitor is much more significant than that of CT unit

insulation. Measurement data indicates that the capacitance variation of the CT unit is less than 0.3%, while that of the ceramic capacitance has a maximum change of 10%. This justifies the above procedure used to calculate the phase shift introduced by the ceramic capacitor at different ambient temperatures.

3.4 Test results

Based on the software simulation and laboratory tests, the tests were performed using optimal measurement parameters (see Chapter 2). The sampling rate was set to 200kS per second and the trigger point set at zero degrees. The three phases of the CT unit insulation were measured and the average value over ten cycles was taken as the measurement result. Typical voltage and current signals obtained are shown in Fig. 3.13, and the harmonic components are shown in Table 3.1.

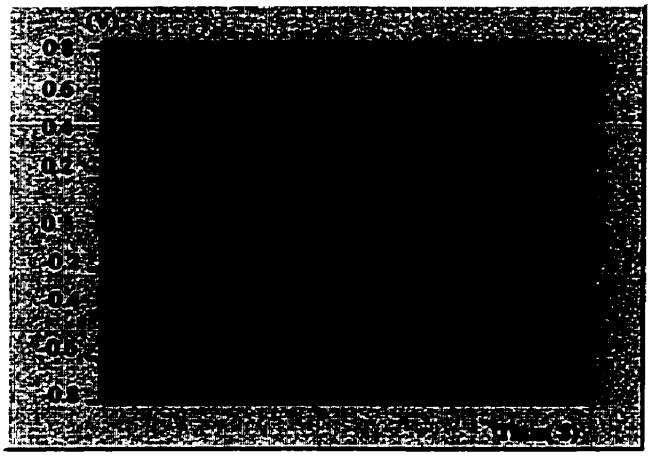

Current signal : ~~ Voltage signal: ···

Figure 3.13 Typical Waveforms of acquired signals (Phase A)

Harmonic components	Phase		
	A (%)	B(%)	C(%)
3^{rd}	0.26	0.20	0.28
5^{th}	0.37	0.30	0.32
7^{th}	0.27	0.28	0.22
9^{th}	0.01	0.01	0.03
11^{th}	0.23	0.10	0.13

Table 3.1 Voltage harmonic components at Dorsey station
(230kV line from Dorsey to St. Leon, Oct 12, 1999)

In order to evaluate the performance of the developed system, measurement of the CT unit insulation was carried out on different days but under similar operating conditions, i.e. it was ensured that the ambient temperature and the capacitance of the ceramic capacitor were the same. The measured results of tanδ are very close, as shown in Fig. 3.14. This proves the reliability of the developed system. Typical measured data

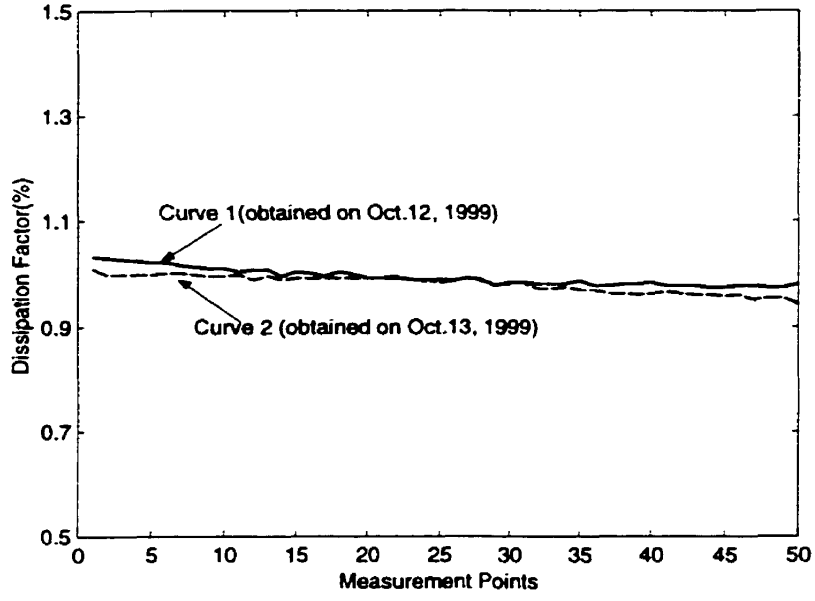

Figure 3.14 Measured results under similar operating conditions
(uncorrected for the phase shift, phase B of the CT unit, Temp: 8.5 °C)

for the three phases before correction for phase shift is shown in Fig. 3.15. Table 3.2 shows corrected data which takes into account of phase shifts introduced by the PT, isolating transformer and the ceramic capacitor.

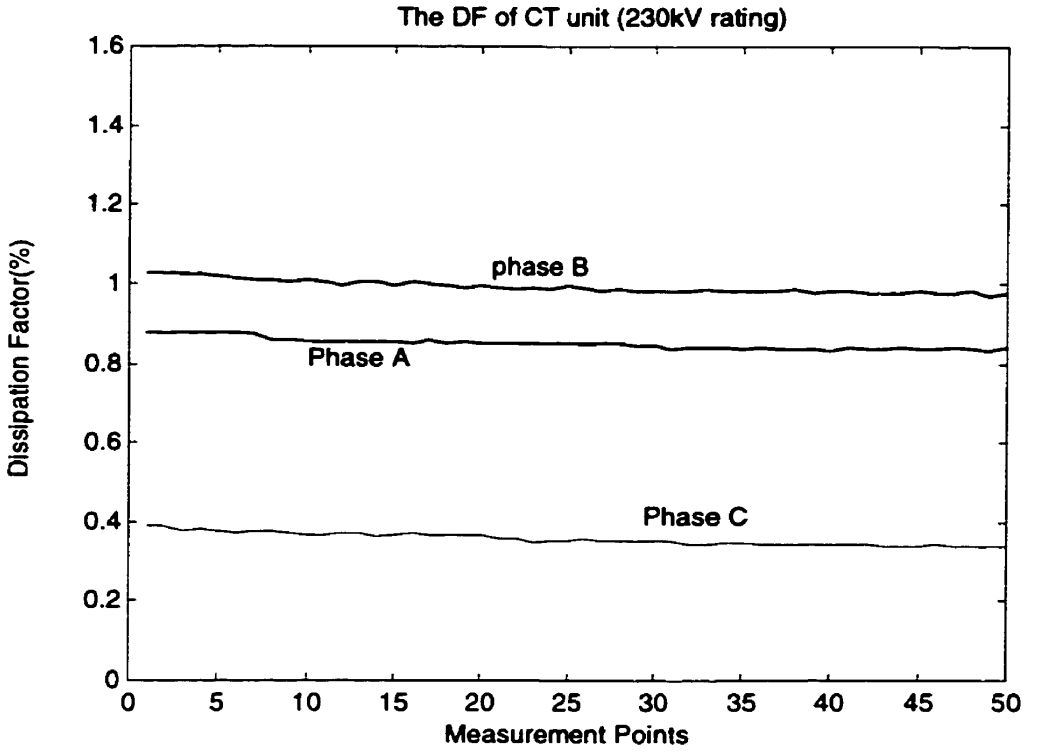

Figure 3.15 Measured Dissipation Factor of the CT unit (uncorrected for phase shift), Oct. 12, 1999

Phase	tanδ (%)	Capacitance (pF)
A	0.428	641.1
B	0.623	665.4
C	0.142	640.7

Table 3.2 On-line measurement results of dissipation factor and capacitance after correction

In order to find the effects of parameters such as load profile and temperature on the results of tanδ, a continuous measurement was carried out over a 24 hour period. The measured data indicated a dramatic change of tanδ and stable values of the capacitance of the CT unit, as shown in Fig. 3.16. By analysis, it is found that the large change of tanδ values is mainly due to the capacitance deviation of the ceramic capacitor. However, the effect of phase shift introduced by the ceramic capacitance could not be accounted for because the procedure set out in section 3.3.2 could not be implemented automatically. Therefore, the tanδ data in Fig. 3.16 does not reflect the real insulation condition of the CT unit.

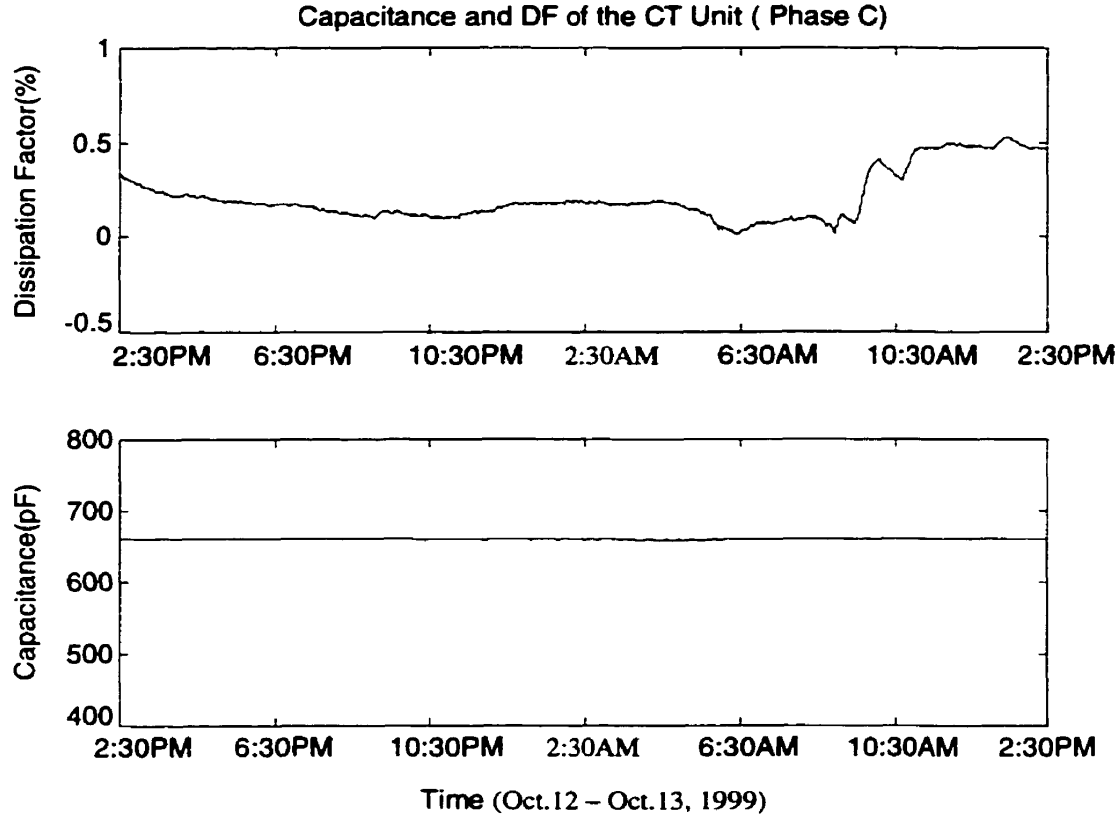

Figure 3.16 Measured data of CT unit for phase C
(uncorrected data, over a 24 hour period)

3.5 Summary

The set-up in this work is different from that in [4] [10] in that the combination of a ceramic capacitor and a shunt resistor was used to acquire the current signal from the test object. It provides for reliable and safe operation. The trade-off is that the capacitance is affected by the ambient environment. A procedure was therefore devised to compensate its effect on the measurement of the tanδ of the CT unit.

The software "Labview" provides powerful support for the data acquisition, signal processing, and graphic user interface. In addition to the values of tanδ and capacitance, the instantaneous values of waveforms can be shown and the harmonic components can be obtained.

The developed system is applicable for the on-line measurement of the insulation of H.V apparatus. The continuous monitoring with the developed system will make it possible to find the effects of seasonal changes and operating conditions on the insulation, provided the phase shift introduced by the ceramic capacitor is compensated for or alternatively it is substituted by a capacitor with a very low temperature coefficient. In combination with other information it will be possible to set up an intelligent system to diagnose the state of insulation and suggest remedial action.

CHAPTER 4

CONCLUSIONS

In the work presented in this thesis, an on-line digital method for measuring dissipation factor and capacitance of high voltage apparatus is presented.

Chapter 1 briefly introduces the history of the insulation diagnostic methods, especially the methods employed to measure dissipation factor and capacitance. In Chapter 2, a developed system based on the proposed digital method is described in detail. Computer simulation and laboratory tests were carried out to evaluate system performance and to find optimum measurement parameters. In addition, a method employing cancellation of capacitive current was investigated for application to high capacitance insulation. Hardening of the measurement system and on-line measurement of the dissipation factor of a 230kV current transformer unit at Manitoba Hydro's Dorsey station are discussed in Chapter 3.

The following conclusions may be drawn:

1. The measurement error can be reduced by increasing the sampling rate; the error saturates after the sampling rate reaches a certain value.
2. The developed digital system can effectively eliminate the effect of voltage harmonics, which causes significant errors in the method of zero-crossing detection.

3. The measurement precision of the developed method is ±0.05%. This precision is obtained by the proper choice of sampling rate, trigger point locations, and averaging the measurements over a number of sampled cycles.
4. The errors in dissipation factor are dependent on the actual values of dissipation factor for the method employing cancellation of capacitive current, when the signals are contaminated with harmonics.
5. The technique that employs cancellation of capacitive current has acceptable accuracy.
6. A stable circuit based on the combination of a ceramic capacitor and the resistive shunt is suggested to derive the current signal from the test object in on-line tests. The effect of the temperature coefficient of the ceramic capacitor has to be compensated for using the method discussed in section 3.3.2. Alternatively, the ceramic capacitor must be replaced by a capacitor with low temperature coefficient.
7. The suggested on-line method can provide safe and reliable operation after compensation for the temperature coefficient of the ceramic capacitor.
8. The developed system based on the proposed digital method is suitable for on-line measurement. In addition to the values of tanδ and capacitance, the instantaneous values of waveforms can be shown and the harmonic components can be obtained.

References

[1] E. Kuffel, W. S. Zaengl, "High Voltage Engineering: Fundamentals", Pergamon Press, 1988.

[2] Joseph J. Kelly, "Transformer Fault Diagnosis by Dissolved-Gas Analysis", IEEE Transactions on Industry Applications, Vol. IA-16, No. 6, pp. 777-782, November/December 1980.

[3] Alexander G. Schlag, "The Recovery Voltage Method for Transformer Diagnosis", Tettex Instruments, 1994.

[4] D. Allan, M. Blundell, K.boyd and D. Hinde, "New Techniques for Monitoring the Insulation Quality of In-service HV Apparatus", IEEE Transactions on Electrical Insulation, Vol. 27, No. 3, pp. 578-585, 1992.

[5] Mark F. Lachman, W. Walter, Philip A. von Guggenberg, "On-line Diagnostics of High Voltage Bushings and Current Transformers Using the Sum Current Method", IEEE Transactions on Power Delivery, PE-471-PWRD-0-03-1999.

[6] N. H. Ahmed, N. N. Srinivas, "On-line Partial Discharge Detection in Cables", IEEE Transactions on Dielectrics and Electrical Insulation, Vol. 5, No. 2, pp. 182-188, April 1998.

[7] R. K. Fricker, "Monitoring HV Insulation Integrity On-line", Transmission and Distribution World, Vol. 48, No. 4, pp. 26-37, April 1996.

[8] Genling Zhu, Jinghan Wang, "Measurement of Tanδ and C of Single Phase Electrical Apparatus of Capacitive Insulation Under Operating Voltage", IEEE International Conference on Properties and Apparatus of Dielectric Materials, pp. 701-703, 1988.

[9] Dr. P. Vujovic, R. K. Fricker, J. A. Ehrich , A. R. Young, "Development of An On-line Continuous Tan (δ) Monitoring System", IEEE International Symposium on Electrical Insulation, pp. 50-53, Pittsburgh, 1994.

[10] Zhang Yan, Jiwen Chai, Yongfa Li , Zhixian Wang, Zhonggui An, Juling Yi, "On-site Automatic Measurement of HV Insulation", IEEE International Conference on Properties and Apparatus of Dielectric Materials, pp. 642-644, 1988.

[11] Zhengkao Zhang, "Digital Technique for On-line Measurement of Dissipation Factor of High Voltage Apparatus", M. Sc. thesis, University of Manitoba, December 1997.

[12] Alessandro Ferrero, Roberto Ottoboni, " High Accuracy Fourier Analysis Based on Synchronous Sampling Techniques", IEEE Transactions on Instrumentation and Measurement, Vol. 41, No. 6, Decemeber 1992.

[13] Xiangxiao Qiu, "Diagnostic Methods to Detect Ageing in MOSA Valve Elements", M. Sc., University of Manitoba, 1995.

APPENDIX A

MEASUREMENT SYSTEM GRAPHIC USER INTERFACE (GUI)

The developed digital measurement system has a user friendly and easy-to-use graphic user interface (GUI), as shown in the following figure. The GUI includes two main sections, i.e. control and display sections, for the measurement of tanδ and capacitance.

Figure A.1 Measurement system graphic user interface (GUI)

In the **Control section,** different measurement parameters can be adjusted to obtain optimal system performance. The control section consists of the following units:

- Shunt resistor control for the scaling of the current signal.
- Voltage ratio control for the scaling of the voltage signal.
- Sampling rate control: variable from 0 to 10M Samples/second.
- Switch for the method employing cancellation of capacitive current and percentage control of the cancellation current magnitude.
- Sampled cycles control.
- Trigger point control: variable from 0 to 90 degrees.

The **Display section** is used for the graphic and digital illustration of the measurement results. It is composed of the following:

- Window to show the acquired waveforms simultaneously (both current and voltage signals) with respect to time.
- Windows to show the measured tanδ and capacitance values with respect to the measurement number. Each measurement in tanδ and capacitance is the average value over a certain cycles.
- Digital display of the voltage harmonics (from DC to 13th harmonic).

APPENDIX B

CALIBRATION OF PHASE SHIFT IN ON-LINE TESTS

1. Phasor diagram for taking into account phase shift in the on-line tests.

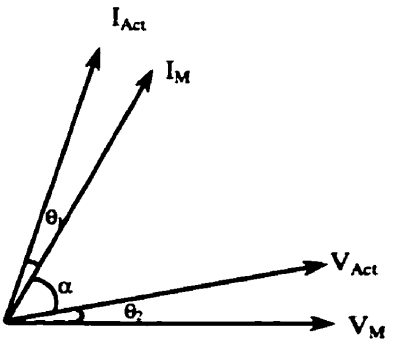

Fig. B.1 Relationship between measured and actual loss angles

Measured loss angle: $\delta_1=90^\circ-(\alpha+\theta_2)$

Actual loss angle: $\delta_2=90^\circ-(\alpha+\theta_1)= \delta_1-\theta_1+\theta_2$

where: θ_1: phase shift in the current signal; θ_2: phase shift in the voltage signal

2. Calculation of phase shift in current signal

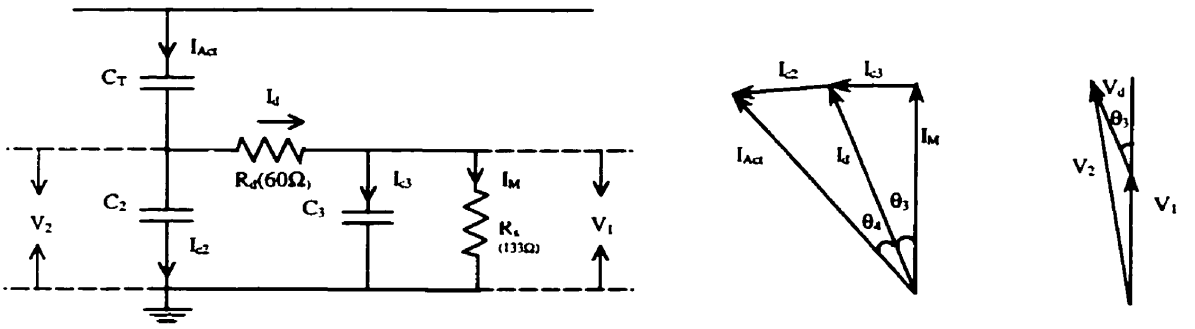

Fig. B.2 Calibration circuit of phase shift in current signal

$\tan\theta_3 = \omega C_3 R_s$; $\tan\theta_4 \approx \omega C_2(R_s+R_d)$;

Total phase shift in current signal: $\theta_1=\theta_3+\theta_4$

Where: C_3, capacitance of the varistor is equal to 12500pF; Values of C_2 is obtained using the technique described in section 3.3.2 (C_{2A}=0.6057μF, C_{2B}=0.6027μF, C_{2C}=0.5795μF, subscript A, B and C refer to the three phases, obtained on Oct.12, 1999).

3. Calculation of phase shift in the voltage signal.

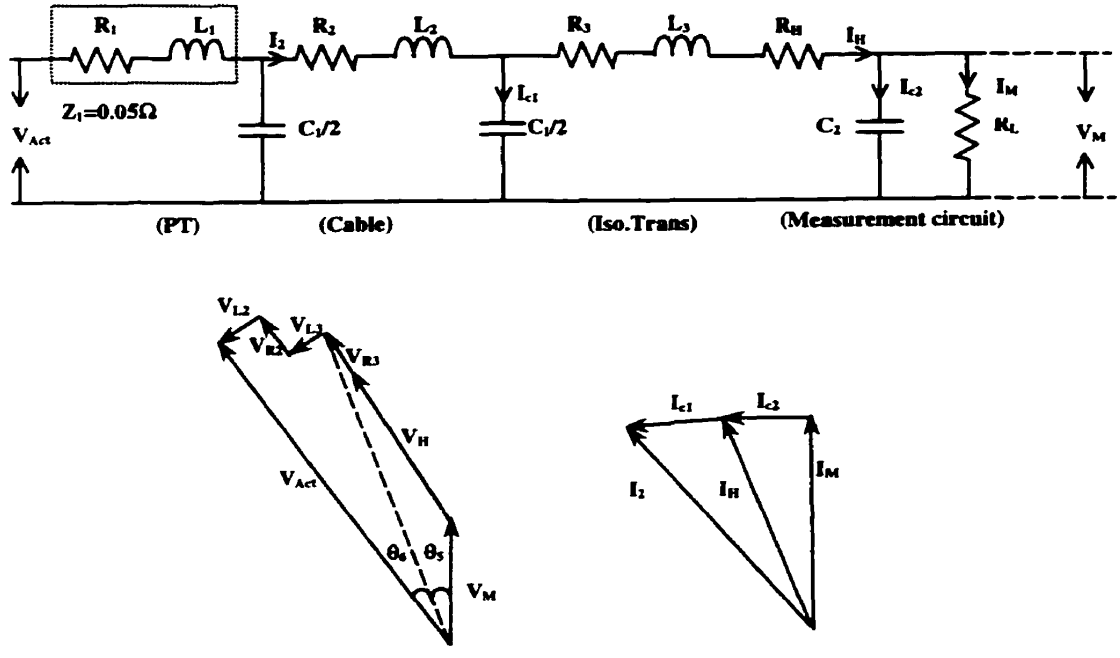

Fig. B.3 Calibration circuit of phase shift in voltage signal

- Cable: 12AWG, 900 foot long, copper, shielded, 4-conductor.

  R_2=1.44Ω, X_2=0.2Ω

  C_{1A}=87912pF, C_{1B}=72603pF, C_{1C}=87174pF [A, B, C refer to the 3 phases]

- Isolating transformer: R_3=0.48Ω, X_3=1.49Ω (See Fig 3.8 in chapter 3)

- Measurement circuit: R_H=10kΩ, C_2 (varistor capacitance)=13500pF, R_L=614Ω (See Fig 3.2 in chapter 3)

$\tan\theta_5 \approx \omega C_2 R_L$; $\tan\theta_6 \approx (X_2+X_3)/(R_H+R_L)$

Total phase shift: $\theta_2=\theta_5+\theta_6$

θ_2 is equal to 0.32% radian or 11 minutes, same in the three phases.

4. Measured data: (No correction implemented to account for phase shift in the voltage signal; calculation of phase shift in the current signal is based on a value of rated value 0.5μF for C_2).

Phase	A	B	C
tanδ (%)	0.88	1.05	0.40

5. Corrected data: (taking into account phase shift in voltage and current signal)

Phase	A	B	C
tanδ (%)	0.43	0.62	0.14
Capacitance (pF)	641.1	665.8	640.7